Mon. Not. R. Astron. Soc. **381,** 245–262 (2007) doi:10.1111/j.1365-2966.2007.12246.x

The *Galaxy Evolution Explorer* UV emission in shell galaxies: tracing galaxy 'rejuvenation' episodes

R. Rampazzo,[1⋆] A. Marino,[1] R. Tantalo,[2] D. Bettoni,[1] L. M. Buson,[1] C. Chiosi,[2] G. Galletta,[2] R. Grützbauch[3] and R. M. Rich[4]

[1]*INAF – Osservatorio Astronomico di Padova, Vicolo dell'Osservatorio 5, 35122 Padova, Italy*
[2]*Dipartimento di Astronomia, Universitá di Padova, Vicolo dell-Osservatorio 2, 35122 Padova, Italy*
[3]*Institut für Astronomie, Universität Wien, Türkenschanzstraße 17, A-1180 Wien, Austria*
[4]*Physics & Astronomy Department, UCLA, Box 951562, 405 Hilgard Avenue, Los Angeles, CA 90025-1562, USA*

Accepted 2007 July 17. Received 2007 July 17; in original form 2007 April 3

ABSTRACT

We present the *Galaxy Evolution Explorer* (*GALEX*) far-ultraviolet (FUV) and near-ultraviolet (NUV) imaging of three nearby shell galaxies, namely NGC 2865, NGC 5018 and NGC 7135 located in low-density environments.

The system of shells and fine structures visible in the optical is detected in the NUV image of NGC 2865 and in both NUV and FUV images of NGC 7135. The NUV image of NGC 5018 does not present shell structures. We detect absorption features in the nuclear region of all three galaxies. NGC 2865 has a nearly flat colour profile with (FUV−NUV) ≈ 2 throughout the whole galaxy. NGC 7135 is blue in the centre (FUV−NUV) ≈ 0 and as red as (FUV−NUV) ≈ 1.5 in the outskirts, including the faint shell-like feature.

The three shell galaxies are members of poor groups of galaxies. We compare *GALEX* NUV observations with available H I large-scale measurements, and determine the UV magnitudes of likely companions. Most of the known (and possible) companions are gas-rich late-type galaxies, suggesting that our shell galaxies inhabit the ideal environment for hosting *rejuvenating* episodes driven by accretion events.

We investigate the ability of the *nuclear GALEX* (FUV−NUV) colour to provide information about *rejuvenation* phenomena in the stellar populations of the shell galaxies. To this aim, we derive from theory the relationship between the Mg2, Hβ, HγA, HδA Lick line-strength indices and the (FUV−NUV) colour. We extend the study to a sample of early-type galaxies in low-density environments which includes shell galaxies and/or galaxies with emission lines in their optical spectra. In the index versus (FUV−NUV) colour diagrams, most of the galaxies are well explained by passively evolving single stellar populations. On the average, ages and metallicities of the galaxies in our sample estimated from optical line-strength indices are consistent with those inferred from the (FUV−NUV) colour. We note that the *GALEX* (FUV−NUV) and (UV−V) colours have different response to age and metallicity. In general, all the colours but for (FUV−NUV) and (FUV−V), become nearly age-insensitive when 1–2 Gyr have elapsed from the last star-forming event. Finally, considering composite stellar population models with a recent burst of star formation, we suggest that the positions of the NGC 7135 and NGC 2865 nuclei in the (FUV−NUV)–Hβ plane could be explained in terms of a recent rejuvenation episode.

Key words: galaxies: elliptical and lenticular, cD – galaxies: evolution – galaxies: formation – galaxies: fundamental parameters – galaxies: interactions.

1 INTRODUCTION

Shell galaxies represent the ideal class of objects to investigate galaxy evolution in the field for several reasons. Two different scenarios for their origin emerge from the rich harvest of

⋆E-mail: roberto.rampazzo@oapd.inaf.it

simulations performed since their discovery in the early 1980s: either a weak interaction between galaxies (Thomson & Wright 1990; Thomson 1991) or merging/accretion events between galaxies of different masses [mass ratios typically 1/10–1/100; Dupraz & Combes (1986); Henquist & Quinn (1987a,b)].

Weak interactions can form long-lasting azimuthally distributed shells through the interference of density waves produced in a thick disc population of dynamically cold stars. However, this requires a cold thick disc, not found in ellipticals. In merging models, shells are density waves formed by infall of stars from a companion during a minor merger. Major merger can also produce shells (Barnes 1992; Hernquist & Spergel 1992; Hernquist & Mihos 1995).

Both scenarios qualitatively reproduce basic characteristics, such as spatial distribution, frequency and shape of observed shell systems (see e.g. Wilkinson et al. 2000, and references therein). Weak interaction models add also clear information about the environment: shells could not be maintained within clusters, as the continuous 'harassment' among galaxies would destroy them.

Shell galaxies indeed avoid the cluster environment and are found in the field with a high frequency (≈16.5 per cent of the early-type galaxy population, Malin & Carter 1983; Schweizer 1992; Reduzzi, Longhetti & Rampazzo 1996; Colbert, Mulchaey & Zabludoff 2001). This suggests that interaction/accretion/merging events have played a significant role in the formation/evolution of the early-type class as a whole.

Using Fabry–Perot observations, Rampazzo et al. (2003) analysed the warm gas kinematics in a few shell galaxies. They found that gas and stars appear to be decoupled in most cases. This evidence suggests an external acquisition of the gas, as predicted by merging models. At the same time, a set of observations showing a clear association between cold (H I/CO) gas and stars challenge present merging models which do not predict it unless cold gas behaves differently from the ionized gas (Schiminovich et al. 1994, 1995; Charmandaris, Combes & van der Hulst 2000; Balcells et al. 2001). Studying the distribution of shell galaxies in the Hβ versus [MgFe] line-strength index plane, Longhetti et al. (2000) show that these systems span a wide range of ages, indicating that among them recent and old interaction/acquisition events are equaly probable. If shells are formed at the same time at which the rejuvenating event took place, shells ought to be long-lasting phenomena. Thus, whereas current studies in literature considers the shell structure surrounding early-type galaxies as a *bona fide* indicator of past accretion/merging events, their formation age and secular evolution are far from being firmly established.

In the above framework we discuss *Galaxy Evolution Explorer* (*GALEX*) observations of three shell galaxies taken from the Malin & Carter (1983) compilation, namely NGC 2865, NGC 5018 and NGC 7135. The galaxies are located in very low density environments and belong to HI rich associations. NGC 2865 and NGC 7135 are part of our *GALEX* proposal (GI04-0030-0059). The NGC5018 data are taken from the *GALEX* archive. The line-strength indices analysis performed by Longhetti et al. (2000) and Annibali et al. (2007) suggests that the above shell galaxies had a recent burst of star formation (SF). The present sample is then not representative of the entire class of shell galaxies (see e.g. Longhetti et al. 2000). Through this pilot study we aim to verify whether these galaxies host ongoing SF and how it distributes across the galaxy.

The plan of the paper is as follows. Section 2 describes the relevant properties of our galaxy sample that could be gathered from literature. Section 3 presents the *GALEX* observations and the data reduction. Results are presented in Section 4 and discussed in Section 5.

2 THE SAMPLE

We collect in Table 1 the main characteristics of the galaxies under examination. As may be deduced from the local galaxy density, $\rho_{(x,y,z)}$ (gal Mpc^{-3}), the galaxies are located in very low density regions of complex galaxy associations (Tully 1988).

(i) *NGC 2865*. According to Jørgensen, Franx & Kjægaard (1992) the galaxy is a *bona fide* elliptical with a surface brightness profile

Table 1. Data for the three shell galaxies observed in this study.

	NGC 2865	NGC 5018	NGC 7135	Reference
Morphological type	E3-4	E3	SA0-pec	[1]
Heliocentric systemic velocity (km s^{-1})	2627 ± 3	2794 ± 15	2640 ± 21	[1]
Adopted distance (Mpc)	35.7	40.9	34.7	[2]
$\rho_{(x,y,z)}$ (gal Mpc^{-3})	0.11	0.29	0.32	[2]
Environment	Antlia-Hydra clouds	Virgo Southern extension	Pisces-Austrinus Spur	[2]
Apparent magnitude and colours				
B_T	12.57 ± 0.14	11.69 ± 0.13	12.79 ± 0.15	[1]
$\langle(B-V)_T\rangle$	0.91	0.92	0.99	[1]
$\langle(U-B)_T\rangle$	0.41	0.48	0.42	[1]
$(J-H)_{2MASS}$	0.65	0.63	0.66	[1]
$(H-K)_{2MASS}$	0.25	0.30	0.22	[1]
Galaxy structure				
Effective surface brightness $\mu_e(B)$	20.20 ± 0.27	20.35 ± 0.25	22.78 ± 0.60	[3]
Diam. effective aperture, A_e (arcsec)	25.0	45.5	62.8	[3]
Average ellipticity	0.17	0.32	0.28	[3]
PA (°)	154.6	99.9	44.9	[3]
Kinematical parameters				
Velocity dispersion σ_0 (km s^{-1}) stars	180 ± 24	240	202 ± 21	[3]
Maximum rotation V_{max} (km s^{-1})	234 ± 30	75±15	78	[3]

References. [1] NED: http://nedwww.ipac.caltech.edu/; [2] Tully (1988) ($H_0 = 75$ km s^{-1} Mpc^{-1}); [3] HYPERLEDA: http://leda.univ-lyon1.fr/.

consistent with a pure $r^{1/4}$ law. At the same time, NGC 2865 is genuinely peculiar: in deep images the galaxy displays a significantly disturbed morphology. The isophote fit reveals boxy isophotes within 40 arcsec and discy isophotes at larger radii (Reid, Boisson & Sansom 1994). The galaxy displays a chaotic system of about seven shells out to 2.5 arcmin (Fort et al. 1986). A westward protrusion, identified as a stellar jet or a polar ring (Whitmore et al. 1990), extends 1 arcmin from its nucleus. Fort et al. (1986) estimate that 11–22 per cent of the total luminosity of NGC 2865 is contained in the shells and in the above described protrusion. Further out, in deep images, a faint loop is visible north-west and a plume or tail-like extension can be seen to the south-east. Nevertheless, Schiminovich et al. (1995) H I observations show that NGC 2865 has no companions of similar luminosity, while two gas-rich dwarfs are seen nearby. The above authors suggest that the galaxy might be the recent (less than 7 Gyr) product of a major disc-disc merger, although the association between gas and stellar fine structure, with gas displaced outward from the stars in projected position, implies gas motions not predicted by any of the current merger scenarios. Using nuclear line-strength indices, Longhetti et al. (1999) suggest that NGC 2865 is among those shell galaxies which are candidates for having a very young stellar component in their spectra: their analysis of both [Ca II] and Hβ line-strength indices provide a luminosity-weighted stellar age lower than 2 Gyr.

(ii) *NGC 5018*. The galaxy is peculiar in two main respects. First Schweizer (1990) classified NGC 5018 as one of his prime candidates for a recent major merger, assigning to it a fine structure Σ parameter of 5.15. The Σ parameter is an empirical measure of the optical disturbance present in a galaxy since its value is given by a combination of the optical strength of ripples, the number of detected ripples, the number of jets, an estimate of boxiness and the presence of X-structures. The higher the value of Σ the higher the morphological disturbance and the probability that the galaxy is *dynamically younger*. Secondly, the nuclear optical spectrum has the weakest Mg2 line-strength index considering its velocity dispersion among the over 400 Es surveyed by Davies et al. (1987). Also unusual is the lack in its UV *IUE* spectrum (Bertola et al. 1993) of a prominent UV-upturn shortwards of λ 2000 Å, that is typical of old, metal-rich spheroids (Burstein et al. 1988). Such an anomalous result inspired some authors to propose a kind of conspiracy, where young stars and heavy dust absorption combine with each other to dilute the underlying Mg2 line-strength index, so as to turn a flat, young-star-dominated UV energy distribution into the observed NGC 5018 UV-weak spectrum (Carollo & Danziger 1994). This scenario, however, is not consistent with the average internal reddening as low as $E(B-V) \sim 0.02$ measured by Buson et al. (2001). The relatively young nature of this object was later confirmed by Leonardi & Worthey (2000), who proposed that NGC 5018 is an old, metal-rich elliptical which has undergone a major accretion event at some recent stage of its evolution. In this framework, the above authors interpret NGC 5018 as an object presently dominated by an acquired stellar population not older than 2.8 Gyr. A slightly different view is proposed by Buson et al. (2004) who suggested that in NGC 5018 the bulk of its stellar population were *formed ex-novo* about 3 Gyr ago, just at the time of a major merging event. Finally Tantalo & Chiosi (2004a) explored the possibility that bulk population of stars in NGC 5018 is old and that its unusually high value of Hβ simply reflects the rejuvenation that occurred about 2 Gyr ago, most likely by a merger which, however, was limited to a minor percentage of the stellar mass.

(iii) *NGC 7135*. Malin & Carter (1983) noted that the galaxy presents 'a curious jet and a shell' and a prominent tail on the opposite side of a sharp curved feature. Keel (1985) classified the galaxy as a merger galaxy with a LINER nucleus. Both the stellar tail and the elongated asymmetric distribution of the ionized gas, detected by Rampazzo et al. (2003) suggest indeed a recent acquisition event. In addition, the inner stellar radial velocity, measured by Longhetti et al. (1998), has a similar profile but shifted by about 200 km s^{-1} with respect to the barycentric velocity of the ionized gas.

Annibali et al. (2007) derive a luminosity-weighted age of 2.2 Gyr for NGC7135, which suggests the presence of a young burst of SF. NGC 7135 is included among the few prototypical galaxies that might have suffered from a nearly radial merger (Aalto & Hüttemeister 2000). Once the effects caused by the stellar burst will be over, NGC 7135 is expected to closely resemble the so-called Medusa galaxy (NGC 4194) as suggested by Rampazzo et al. (2003).

In conclusion, there is evidence that all the three galaxies might have undergone recent (2–3 Gyr) *rejuvenation* episodes. The correlation between the onset of SF and the event that triggered the formation of the shell structure could be further investigated using ultraviolet morphology and photometry [i.e. near-ultraviolet (NUV) and far-ultraviolet (FUV) *GALEX* observations].

3 OBSERVATIONS AND DATA REDUCTION

The *GALEX* mission and instruments are fully described in Martin et al. (2005) and Morrissey et al. (2005). The observing logs, including exposure times, for each galaxy are provided in Table 2. The spatial resolution of the images is $\approx$4.5 and 6.0 arcsec full width at half-maximum (FWHM) in FUV (1350–1750 Å) and NUV (1750–2750 Å), respectively, sampled with 1.5×1.5-arcsec^2 pixels.

Two galaxies, namely NGC 2865 and NGC 7135, have been imaged with *GALEX* by means of dedicated observations awarded to our team. The NUV and FUV data for NGC 5018 have been taken from the *GALEX* archive: the FUV image is part of the All-Sky Survey (AIS). Full-resolution images in the NUV and FUV bands are shown in Fig. 1. The quality of the images varies significantly as the exposure time ranges from the NUV image of NGC 2865, the results of the co-adding of several images for a total exposure time of $\approx$16 ks, to the FUV image of NGC 5018 with 118 s.

Our first analysis addresses a morphological study of the galaxy structures. In order to enhance the signal-to-noise ratio (S/N) in

Table 2. Journal of the *GALEX* observations.

Name	NUV exposure (s)	FUV exposure (s)	Observing date	PI
NGC 2865	16 269	2567	2004-12-22	D. Bettoni
NGC 5018	12 38*	118	2005-05-14*	J. van Gorkom*
NGC 7135	1693	1693	2004-10-15	D. Bettoni

Note. The observing date and the PI labelled with an asterisk refer to the NUV observation of NGC 5018.

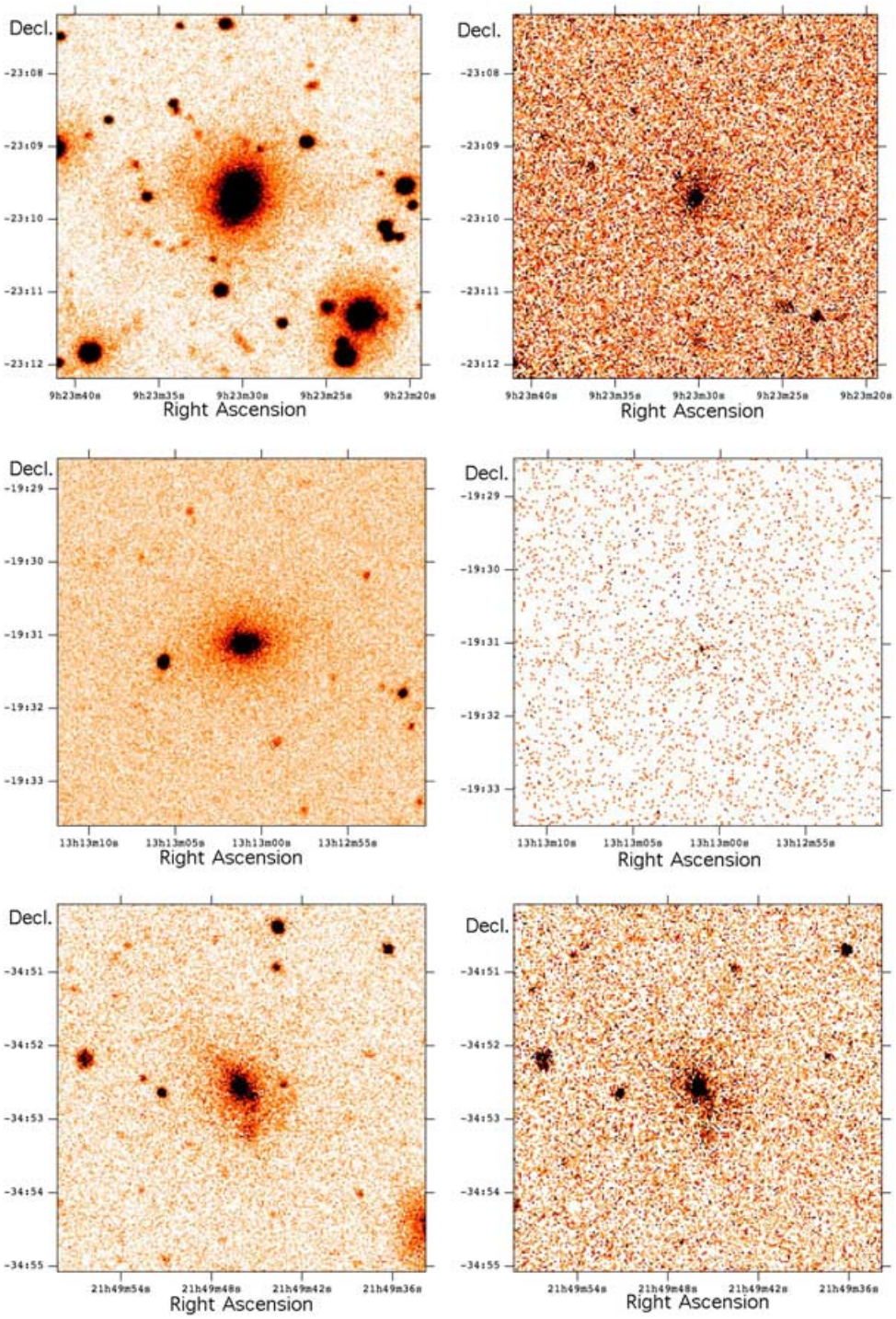

Figure 1. NGC 2865 (top panels), NGC 5018 (middle panels) and NGC 7135 (bottom panels) full-resolution, 5 × 5-arcmin^2-wide *GALEX* NUV (left-hand panels) and FUV (right-hand panels), background-subtracted images in counts pixel^{-1} s^{-1}.

the galaxy outskirts and to bring into evidence possible faint structures in the UV emission, we used both the adaptive kernel smoothing algorithm available in IRAF[1] and ASMOOTH (Ebeling, White & Rangarajan 2006). For each individual pixel the algorithm increases the smoothing scale until the S/N within the kernel reaches a preset value. Thus, noise is suppressed very efficiently, while at the same time the real structure, that is, signal that is locally significant at the selected S/N level, is preserved at all scales. In particular, extended features in noise-dominated regions are visually enhanced (see Figs 2–4).

Surface photometry (Fig. 6) was carried out, on the background-subtracted images, with the ELLIPSE fitting routine in the STSDAS package of IRAF and with the GALFIT package (Peng et al. 2002).

[1] IRAF is distributed by the National Optical Astronomy Observatories, which are operated by the Association of Universities for Research in Astronomy, Inc., under cooperative agreement with the National Science Foundation.

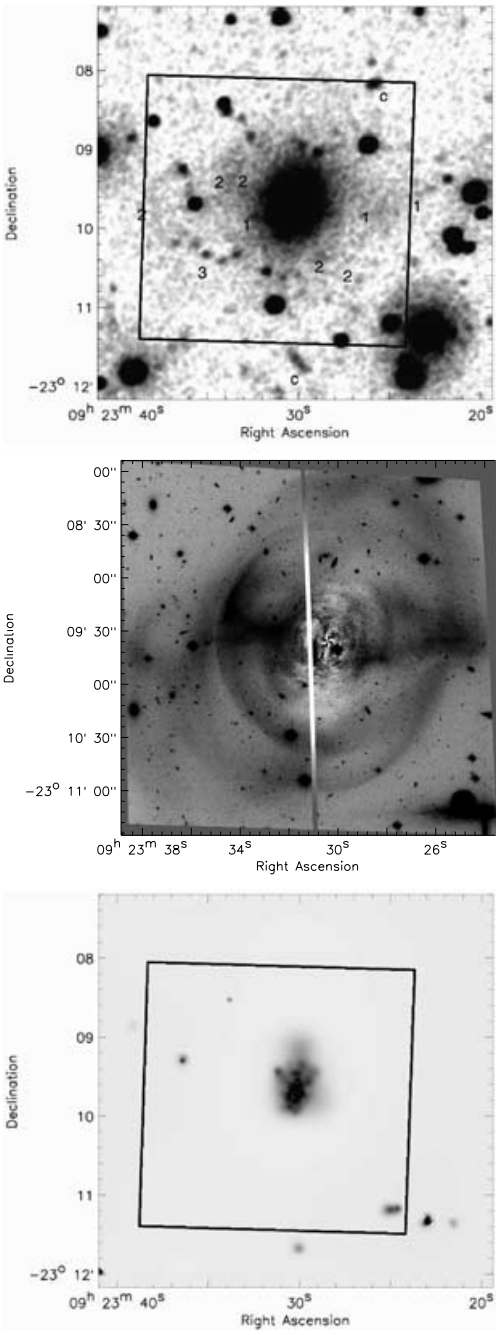

Figure 2. NGC 2865. Top panel: *GALEX* NUV image (FOV = 5 × 5 arcmin^2). The image has been smoothed with an adaptive filter to enhance the outer fine structures. We used for comparison the *HST* ACS *F606W* image of NGC 2865 (FOV = 3.5 × 3.5 arcmin^2) (middle panel) where the main body of the galaxy has been subtracted, revealing a complex fine structure and a central dust system. On the NUV image, we labelled the north-east and north-west protrusions (1) and the shell system (2) visible in the *HST* ACS FOV (see Fort et al. 1986, also see fig. 4 in the quoted paper). We further labelled with 3 a chain of possibly background galaxies barely visible in the optical band and with c the galaxies indicated as 'companions' in Fort et al. (1986). For the faint FUV image bottom panel), we used the ASMOOTH (adaptive Gaussian kernel) filter with $\tau_{\rm min} = 3$. The box in the NUV and FUV images marks the *HST* ACS FOV.

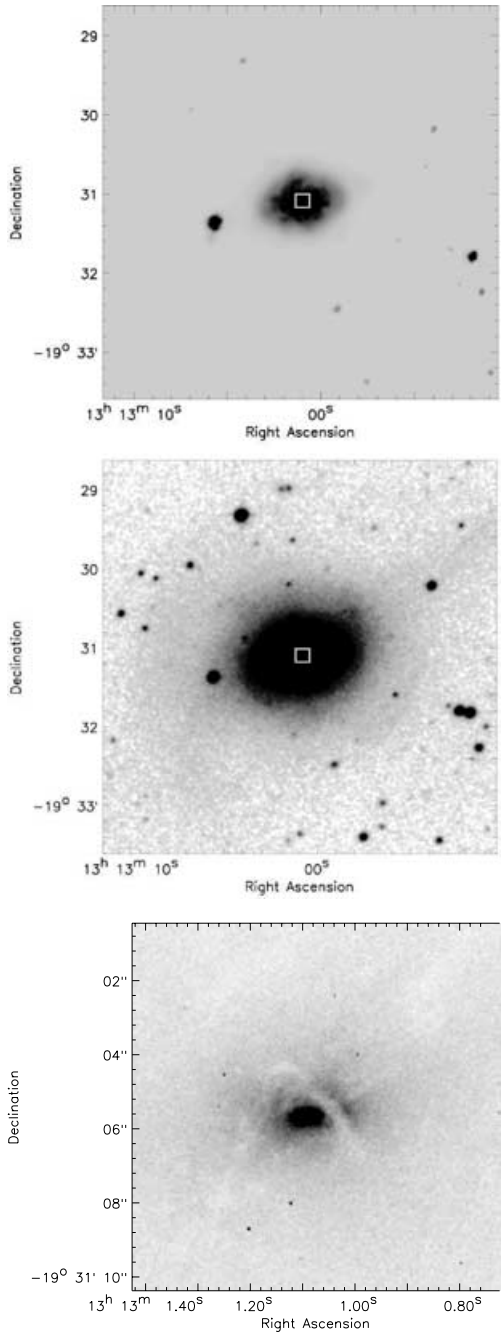

Figure 3. NGC 5018. Top panel: *GALEX* NUV (5 × 5–arcmin^2) image after the application of ASMOOTH filter with $\tau_{\rm min} = 7$. Middle panel: UKSTU Schmidt image with the same FOV as the *GALEX* NUV image. Bottom panel: UV *F336W* (10 × 10-arcsec^2) image from *HST* ACS which reveals the complex system of dust within this galaxy. The box in the NUV and UKSTU images marks the *HST* ACS FOV.

The necessary photometric zero points were taken from Morrissey et al. (2005). AB magnitudes, photometric errors and FUV−NUV colours were determined from the original unsmoothed data. ELLIPSE computes a Fourier expansion for each successive isophote (Jedrzejewski 1987), resulting in the surface photometric profiles. GALFIT was used to perform a bulge-disc decomposition – if needed – and to determine the parameters of the Sersic profile fitted to the bulge of the galaxies. The Sersic profile is a generalisation of the de Vaucouleur law with $\mu(r) \sim r^{1/n}$, where n is a free parameter

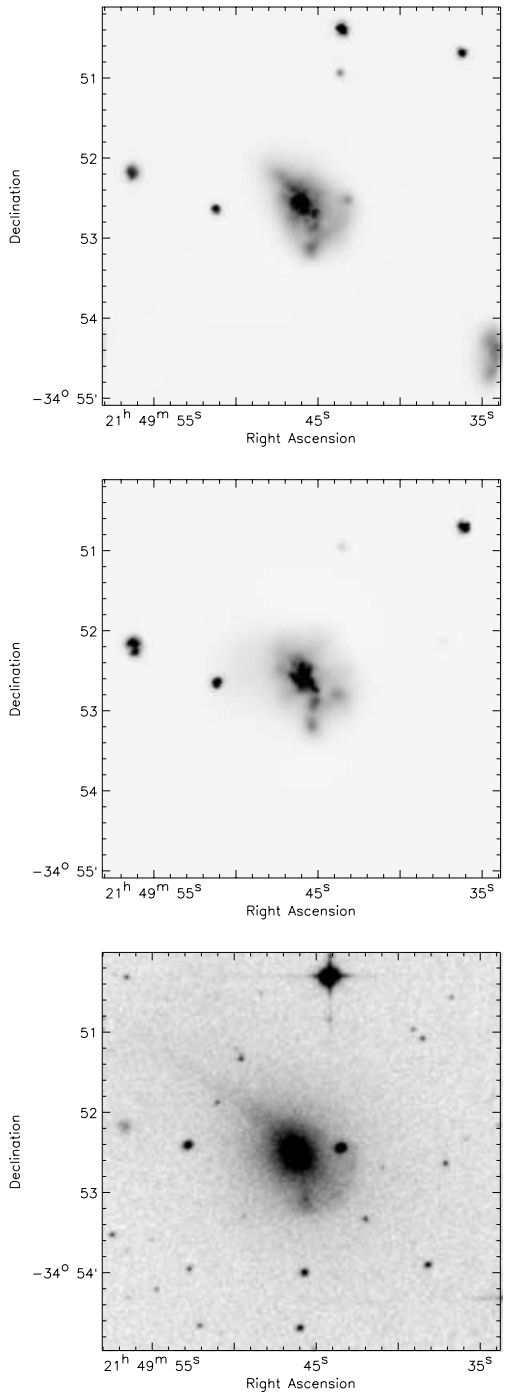

Figure 4. *GALEX* UV and optical images in a 5×5-arcmin^2 field around the NGC 7135 galaxy. Top and middle panels: NUV and FUV images obtained with ASMOOTH for $\tau_{\rm min} = 8$ and 4, respectively. The contrast of the FUV image has been enhanced in order to show the extension of the emission. Bottom panel: UKSTU Schmidt image.

(Sersic 1968), otherwise named the Sersic parameter. The profile is sensitive to structural differences between different kinds of early-type galaxies and thus provides a better fit to real galaxy profiles. GALFIT was also used to search for fine structures on the *HST* ACS *F606W* image of NGC 2865 obtained from the *HST* archive (see Fig. 2, central panel).

We finally analysed the colour distribution across the galaxies. The NUV and FUV images have been scaled to the same spatial resolution in order to avoid spurious colour gradients in the inner parts (Fig. 6).

4 RESULTS

4.1 Galaxy morphology in NUV and FUV

(i) *NGC 2865*. The extension of NUV emission (Fig. 2, top panel) is comparable with that of the optical image, whereas the FUV emission, obtained with a much shorter exposure time (see Table 2), shows up only in the central regions of the galaxy.

We attempted to enhance the fine structure in both NUV and FUV images using adaptive filters. While the FUV image is dominated by the presence of the dust visible in the optical image (see the central panel of Fig. 2), several of the fine structures detected in this latter are also discernible in the NUV image. Both 'protrusions' in the western and eastern sides of the galaxy (evident in the *HST* ACS optical image) and some of the shells (labelled 1 and 2, respectively, in the top panel) are detected. An external shell at about 2 arcmin east of the nucleus is barely visible both in the NUV and in the *HST* ACS image.

The field is crowded with faint, possibly background galaxies. The two galaxies, indicated as 'Companions' in the sketch of fine structure by Fort et al. (1986, see their fig. 4) are detected in NUV and labelled with *c*. The coordinates of the northern object, catalogued as 2MASX J09232585−2308093, are RA $9^\circ 23' 25\farcs 8$, Dec. $-23^{\rm h}\,^{\rm m}08\fs09$. The magnitude is mag $_{\rm NUV} = 22.37 \pm 0.08$. The southern uncatalogued object is located at RA $9^{\rm h}23^{\rm m}29\fs97$, Dec. $-23^\circ 11' 41\farcs 9$. The magnitude is $\rm mag_{NUV} = 21.09 \pm 0.04$.

A chain of bright NUV sources in the East side of NGC 2865 (indicated with 3 in the top panel of Fig. 2) has a counterpart in some optically faint galaxies, barely detectable in the *HST* ACS *F606W* image. From west to east, we identify the following galaxies: (a) RA $9^{\rm h}23^{\rm m}33\fs4$, Dec. $-23^\circ 10' 20\farcs 2$, $\rm mag_{NUV} = 20.86 \pm 0.07$, (b)RA $9^{\rm h}23^{\rm m}34\fs2$, Dec. $-23^\circ 10' 24\farcs 9$, $\rm mag_{NUV} = 23.01 \pm 0.18$, (c) RA $9^{\rm h}23^{\rm m}35\fs1$, Dec. $-23^\circ 10' 20\farcs 1$, $\rm mag_{NUV} = 22.88 \pm 0.16$, (d) RA $9^{\rm h}23^{\rm m}35\fs7$, Dec. $-23^\circ 10' 11\farcs 7$, $\rm mag_{NUV} = 22.21 \pm 0.13$, and (e) RA $9^{\rm h}23^{\rm m}36\fs7$, Dec. $-23^\circ 10' 11\farcs 3$, $\rm mag_{NUV} = 22.08 \pm 0.12$. No measurements of redshift are available for these galaxies.

(ii) *NGC 5018*. The galaxy is characterized by the presence of a complex dust–lane system in the inner parts also visible in the *HST* ACS *F336W* passband which is shown in the bottom panel of Fig. 3. In order to explore the galaxy fine structure we applied the adaptive smoothing technique to the image. However, the low signal does not allow us to reveal any detail of the shell structure sketched in the optical by Fort et al. (1986) (see their fig. 5).

(iii) *NGC 7135*. Contrary to the previous cases, the fine structures visible in the optical DSS image are also revealed both in the NUV and in the FUV images (see Fig. 4, top and mid panels). Specifically, the south-west shell as well as the faint plume extending from the galaxy centre towards the South are clearly visible. In the NUV image, the filamentary tidal tail in the NW direction of the galaxy nucleus visible in the optical image is also seen. This feature makes NGC 7135 a possible analog of the 'Medusa' galaxy, NGC 4194, (see Rampazzo et al. 2003).

Both *GALEX* images suggest the presence of dust in the galaxy nucleus.

4.2 NUV and FUV photometry

Fig. 5 shows the colour (FUV−NUV) maps of NGC 2865 and NGC 7135. The NUV and FUV luminosity profiles of NGC 2865 and

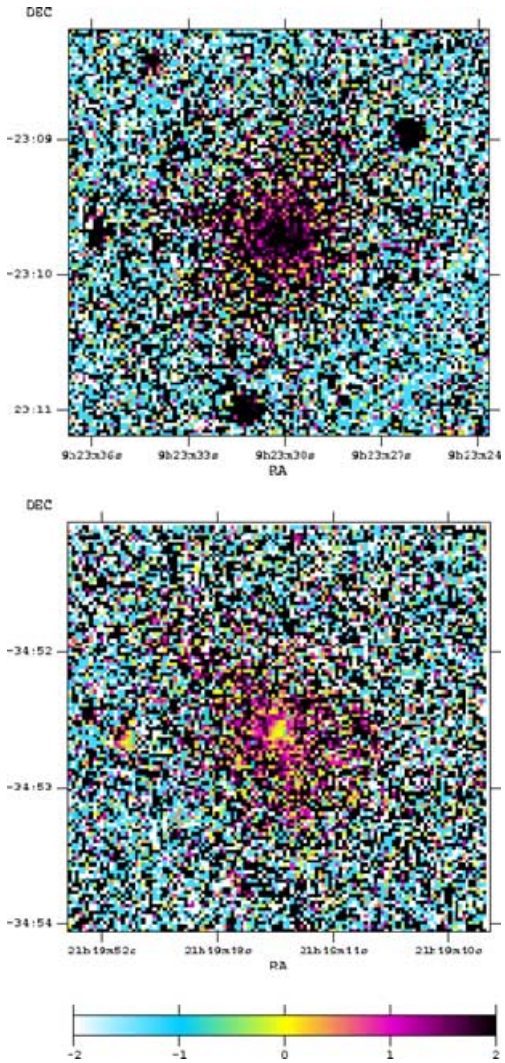

Figure 5. *GALEX* FUV−NUV 2D maps of NGC 2865 (top panel) and NGC 7135 (bottom panel). The colour–colour (FUV−NUV) maps of NGC 2865 and NGC 7135 are derived using NUV and FUV images of equivalent exposure time.

NGC 7135 and the NUV profile of NGC 5018 are shown in Fig. 6. Due to the low expousure time, we do not show the luminosity profile of NGC 5018 in FUV because the S/N is very low. We present also the *F606W* and *F336W* luminosity profiles of NGC 2865 and NGC 5018, respectively. The related colour profiles are plotted in the bottom panels of Fig. 6.

NGC 2865 has a nearly flat and red colour profile with (FUV−NUV) $\approx$ 2 throughout the galaxy. NGC 7135 is quite blue in the centre (FUV−NUV) $\approx$ 0 and becomes as red as (FUV−NUV) $\approx$ 1.5 in the outskirts including the region where the faint plume and the shell-like feature are present.

In Table 3, we present the salient photometric data: the effective radius r_e, that is, the radius containing half of the total galaxy light, the Sersic index, n, the total magnitude computed from the surface photometry in the FUV and NUV bands and the global (FUV−NUV) colour.

The r_e values obtained in the NUV and the FUV bands for NGC 2865 are different. The two images have been obtained with different exposure times (see Table 2). The better determined value of r_e in the NUV band is consistent with that estimated from the *F606W* *HST* ACS optical image and in agreement with the *B*-band values reported in De Vaucouleurs et al. (1991).

Both in NGC 2865 and in NGC 7135, we measured different values of the Sersic index n in the NUV and FUV bands (see Table 3). The fit is very sensitive to the profile structure. The FUV and NUV luminosity profiles of NGC 7135 appear to be really different throughout the galaxy as measured by their very different Sersic indices n. In the *F606W* image the Sersic index we obtained for NGC 2865 is $n = 1.8$ consistent both with NUV and with FUV values although in the optical image the presence of fine structures influences more strongly the determination of the luminosity profile than in the NUV and FUV images.

NGC 2865 and NGC 7135 show quite different (FUV−NUV) gradients. Recent simulations of chemo-dynamical evolution of elliptical galaxies (including radiative cooling, SF, feedback from Type II and Ia supernovae, stellar winds and chemical enrichment) performed by Chiosi & Carraro (2002), Kobayashi (2004) and Merlin & Chiosi (2006) show strong radial metallicity gradients in dissipationless and monolithic collapse of galaxy formation, respectively. Much shallower gradients are foreseen if galaxies formed through major mergers. From an observational point of view, both NGC 2865 and NGC 7135 colour profiles are to some extent peculiar since ellipticals show, on the average, a reddening of the colours towards the centre (Peletier 1990) as a consequence of a metallicity gradient. On the ground of the lack of correlation between the metallicity–σ_c and the [α/Fe]–σ_c relations (σ_c and [α/Fe] are central velocity dispersion and the α- enhancement, respectively), Annibali et al. (2007) suggest that the young ages measured for some of their early-type galaxies are not the result of a more prolonged SF. In particular, for NGC 7135, they support the idea that the young age measured is due to a recent rejuvenation episode of which the presence of the shells morphology is a further indication. In the following sections, we will investigate if the above hypothesis is also supported by our *GALEX* data.

5 DISCUSSION

5.1 Shell galaxies and their environment

The *GALEX* wide field of view (FOV) allows us to study the environment of shell galaxies. Table 1 reports the low galaxy density estimated by Tully (1988) for our objects. Given that shell galaxies are typically found in low-density environments, both their high frequency (16.5 per cent of field Es show shells) and their most likely interpretation (the result of a recent accretion/merging event) suggest that these systems could trace the typical secular evolution of early-type galaxies within poor, loose groups.

In this context, the S0 galaxy NGC 474 with a large shell system and member of Arp 227 together with the spiral NGC 470, could be a typical example. Rampazzo et al. (2006) argued that both the large shell system (likely due to an accretion episode) and the gas-rich, faint late-type companions detected in H I south of NGC 470 would suggest that Arp 227 is a 'poor group in evolution'. Therefore, it could show us how the evolution proceeds in low-density environments. Indeed, both the (M_{H_2}/M_{Hi+H_2}) and the L_X/L_B ratios for NGC 470 are indistinguishable from those of isolated galaxies while the X-ray emission of NGC 474 is barely detected by *XMM–Newton* observations Rampazzo et al. (2006) at odds with evolved groups and/or so called 'fossil groups' (Sansom, Hibbard & Schweizer 2000). Arp 227 could be a snapshot of a group in early evolutionary phases, the drivers of which are the accretion of

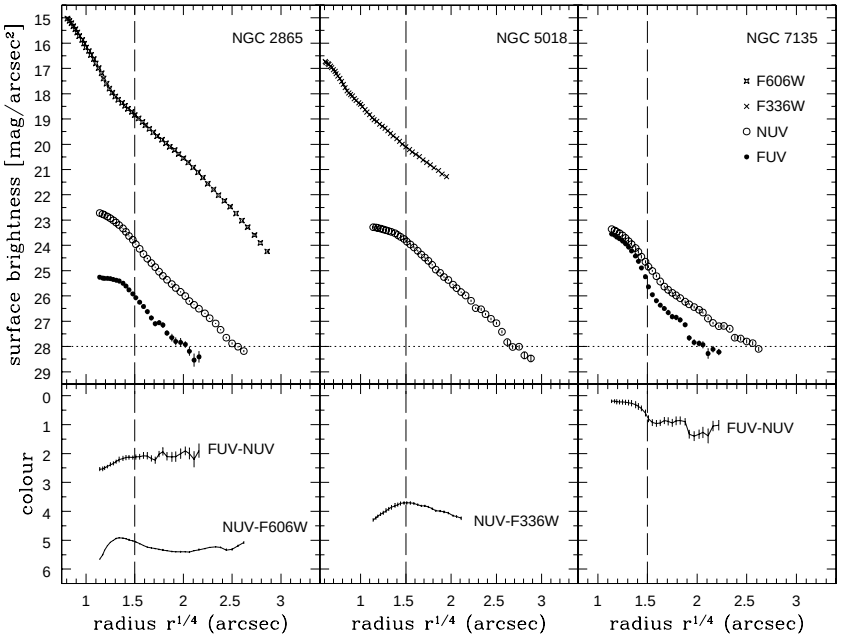

Figure 6. Top left-hand panel: *GALEX* UV and optical surface brightness profiles of NGC 2865. Top middle panel: NUV and *GALEX* NUV luminosity profiles of NGC 5018. Top right-hand panel: *GALEX* UV surface brightness profile of NGC 7135. Bottom panels: colour profiles, from the left-hand to right-hand side, of NGC 2865, NGC 5018 and NGC 7135. With the vertical dashed line at 5 arcsec the approximate FWHM of the *GALEX* point spread function is indicated.

Table 3. Summary of the *GALEX* photometric data.

	NGC 2865	NGC 5018	NGC 7135
r_e^{NUV} (arcsec)	27	34	52
r_e^{FUV} (arcsec)	37		52
n_{Sersic} (NUV)	1.5	3.3	2
n_{Sersic} (FUV)	2.2		4
m_{FUV}^{tot} (1530 Å)	18.59 ± 0.14		17.85 ± 0.25
m_{NUV}^{tot} (2310 Å)	16.84 ± 0.10	16.70 ± 0.14	16.87 ± 0.13
$(FUV-NUV)^{tot}$	1.76 ± 0.23		0.99 ± 0.38

faint companions and the ongoing large-scale interaction between the dominant members NGC 470 and NGC 474.

Following this hypothesis we looked for the large-scale distributions of H I available in the literature that could be associated to our shell galaxies and to possible companions. *GALEX* FUV and NUV data will enrich the picture providing us with the SF status of the member galaxies.

Fig. 7 shows the overlay of the NGC 2865 H I observations by Schiminovich et al. (1995) with our *GALEX* NUV image. The NUV image offers the same indications about the association of fine structure and H I emission as the optical image. The atomic gas seems to be associated with the outermost east shell of NGC 2865, while a break is present in the centre of the galaxy and in the position of the West protrusion.

Contrary to the case of the DSS image (Schiminovich et al. 1995, see their fig. 1b), in our deep NUV image (Fig. 7) it is only possible to guess both the large north-west stellar loop present in the optical image and the faint ribbon that projects outwards to the south-east. Along the latter we note, however, an arc-like increase of the NUV luminosity without any obvious optical counterparts in the DSS image.

The H I map shows that there is at least a companion 5.7 arcmin south-east of NGC 2865, namely FGCE 745 whose *GALEX* magnitudes are mag $_{NUV} = 18.77 \pm 0.01$ and mag $_{FUV} = 19.34 \pm 0.04$. The $(FUV-NUV) = 0.57 \pm 0.04$ colour is consistent with a late-type classification (Gil de Paz et al. 2006). The optical systemic velocity of NGC 2865 is 2627 ± 3 km s^{-1}. The H I detection by Schiminovich et al. (1995) indicates that the systemic velocity of FGCE 745 is $\approx$2725 km s^{-1}. More recently, Mattews & van Driel (2000) measured a systemic velocity of 2480 ± 14 km s^{-1} for FGCE 745 suggesting that the galaxy is connected to the NGC 2865 South-Est H I tail.

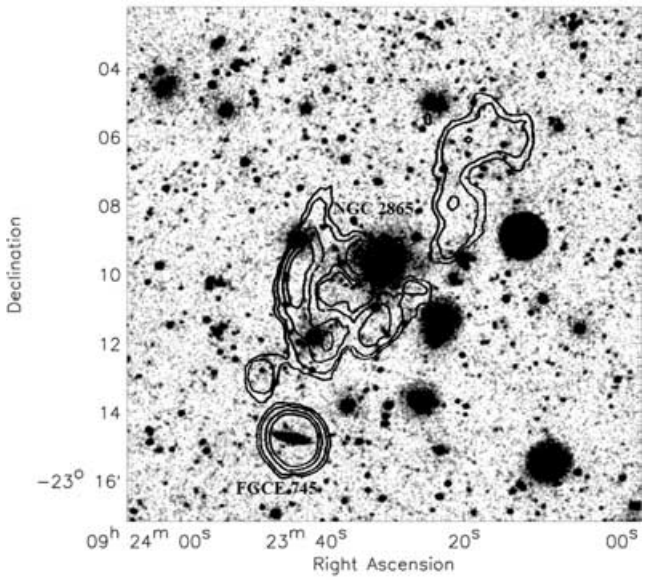

Figure 7. NGC 2865. VLA B+C array, 20-arcsec resolution H I observations performed by Schiminovich et al. (1995) overlaid on the *GALEX* NUV image. The FOV is 13×13 arcmin^2. The galaxy south-east of NGC 2865 is FGCE 745.

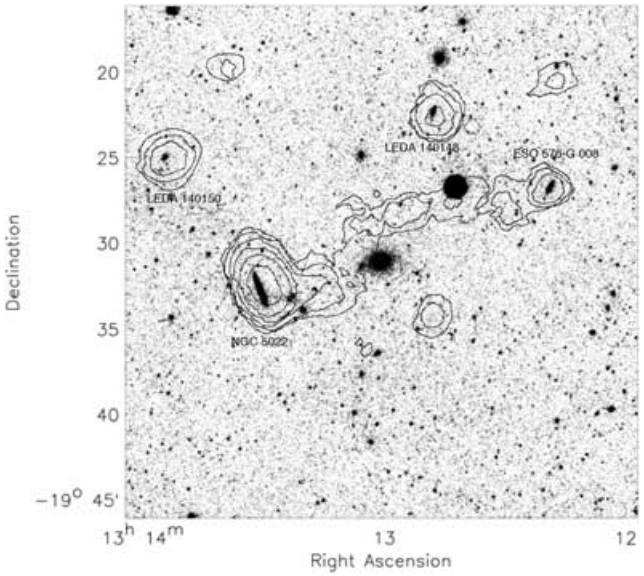

Figure 8. NGC 5018. H I observations overlaid on the *GALEX* NUV original adaptively smoothed image. The FOV is 30×30 arcmin^2. The H I image obtained with the VLA C+D array has a resolution of 60 arcsec (Kim et al. 1988). We label in the figure the galaxies that H I reveals to belong to the groups around NGC 5018. The radial velocity interval of galaxies labelled in the figure, including NGC 5018 at the centre of the field, is $\Delta V \approx 420$ km s^{-1}.

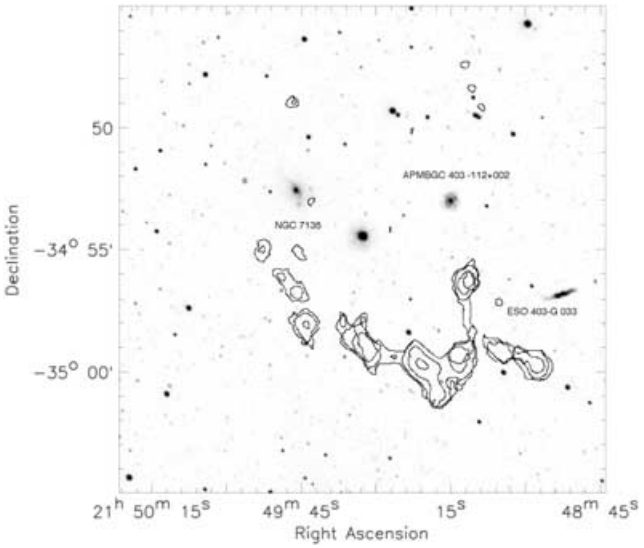

Figure 9. NGC 7135. H I observations overlaid on the *GALEX* NUV original adaptively smoothed image. The FOV is 20×20 arcmin^2. The H I image obtained with the VLA C+D array has a resolution of 60.4×43.2 arcsec^2 (Schiminovich et al. 2001). Galaxies west and south-west of NGC 7135 are APMBGC 403 −112+002 (4831 km s^{-1} from NED that is not bound to NGC 7135) and ESO 403-G 033 (redshift unknown), respectively.

Also the environments of NGC 5018 and NGC 7135 are quite rich in cold gas. Fig. 8 shows the H I image of the field containing NGC 5018 obtained with VLA C+D-array by Kim et al. (1988). There are four H I rich galaxies physically associated to this *bona fide* elliptical, namely NGC 5022 ($V_{\rm hel} = 3001 \pm 8$ km s^{-1} ; mag $_{\rm NUV} = 17.12 \pm 0.01$), ESO 576-G 008 ($V_{\rm hel} = 2691 \pm 39$ km s^{-1} ; mag $_{\rm NUV} = 18.10 \pm 0.02$), LEDA 140148 ($V_{\rm hel} = 3110$ km s^{-1} ; mag $_{\rm NUV} = 17.82 \pm 0.03$), and LEDA 140150 ($V_{\rm hel} = 2732$ km s^{-1} ; mag $_{\rm NUV} = 19.61 \pm 0.06$). According to Kim et al. (1988), there is a clear indication of interaction between NGC 5018 and the spiral companion NGC 5022 from which the gas appears to be flowing towards NGC 5018. The above authors report also about the presence of several blobs of H I, which are marginally detected within a few arcminutes from the optical centre of NGC 5018, and of other three H I features in the group which are not associated with any visible galaxy.

Schiminovich et al. (2001) report the presence of a puzzling, large H I filamentary structure nearby NGC 7135. In the field of NGC 7135 shown by Fig. 9 are present two galaxies of comparable size: APMUKS(BJ) B214615.65–350701.6 and ESO 403–G 033 to the west and south-west of the galaxy, respectively. The former is not associated to NGC 7135 since it has $V_{\rm hel} = 4831$ km s^{-1}. No redshift measures are available for the second object. Neither the FUV nor the NUV images show objects possibly associated to the H I filamentary structure.

5.2 Do shell galaxies host a recent starburst?

Longhetti et al. (2000) studied the Hβ versus [MgFe] plane trying to infer the age of the stellar population in shell galaxies comparing their line-strength indices with those of a sample of interacting and *normal* early-type galaxies. In the above plane, shell galaxies show the same distribution of *normal* early-type galaxies, although a number of shell galaxies and pairs have a much stronger Hβ. Longhetti et al. (2000) suggest that the scatter in the Hβ versus [MgFe] plane could be due to a common origin, perhaps a secondary episode of SF after their formation. The explanation comes naturally for shell (and pair galaxies) where the signatures of interaction are evident. The shape of the distribution of the line-strength indices in the Hβ versus [MgFe] plane suggests the presence of an effect of a metal enrichment that always accompany SF. Longhetti et al. (1999) further suggest that, if the last star-forming event is connected to the formation of the shell system as expected from simulations, the shells ought to be a long-lasting phenomenon since star-forming events that occurred in the nuclear region of shell galaxies are statistically old (from 0.1 up to several Gyr). It is worth mentioning here the study by Tantalo & Chiosi (2004b) who added another dimension to the problem, that is, the effect of the degree of enhancement in α-elements in the abundance patterns. They argued that part of the scatter in Hβ could reflect the intrinsic variation of α-enhancement from galaxy to galaxy existing in old populations of stars due to different SF histories rather than a dispersion in age caused by more recent star-forming episodes.

Based on these premises, we investigate whether the *GALEX* data may confirm or disprove the case that shell galaxies hosted a recent star burst event. Given that UV colours are considered to be particularly suited to identify very young stellar populations and their distribution inside interacting galaxies (see e.g. Hibbard et al. 2005), to (FUV−NUV) we also add the UV-optical colours. There is, however, an important point to keep in mind while dealing with UV colours is that there is possibility that high-metallicity, old stars (age $\geqslant 10^{10}$ yr and metallicity $Z \simeq 3\,Z_{\odot}$) likely to be present even in small percentages in early-type galaxies could affect the (FUV−NUV) colours. The evolved stars in metal-rich populations [extremely horizontal branch (HB) and asymptotic giant branch (AGB) manqué] are the proposed source of the UV excess in quiescent early-type galaxies (Bressan, Chiosi & Fagotto 1994) and any modelling of SF must take this population into consideration, see Bressan et al. (1994) for a detailed discussion on the subject. Fortunately,

we can consider additional clues [presence of dust and gas, dynamics, overall spectral energy distribution (SED)] in interpreting the results.

Our shell galaxies are *dynamically young* objects and belong to environments containing fresh gas in the ionized, neutral and molecular forms. However, the spatial distribution of the gas changes from galaxy to galaxy. Only for NGC 7135 is there some indication in the literature for ongoing gas re-fuelling. In the centre of this galaxy Rampazzo et al. (2003) detected in the Hα emission line the presence of an ionized gaseous component for a total extension of $\approx$20 arcsec, elongated in the southwest direction in correspondence to the FUV emission (Fig. 4, middle panel). The ionized gas and the stars differ significantly in systemic velocity (see Section 2) suggesting that the gas likely originates from an interaction/accretion episode suffered by the galaxy.

For our three galaxies estimates of the mean luminosity-weighted ages have been derived from optical line-strength indices by Longhetti et al. (1999), Leonardi & Worthey (2000), Longhetti et al. (2000), Rampazzo et al. (2005), and Annibali et al. (2007). For comparison we consider here the set of early-type galaxies analysed by Rampazzo et al. (2005), Annibali et al. (2006), and Annibali et al. (2007). These galaxies are characterized by (i) the presence of ionized gas, (ii) their location in low-density environments, also typical of shell galaxies, and (iii) the presence of dynamical/morphological peculiarities in a high percentage of them. Finally, there are also a few additional shell systems. In addition to the three galaxies of this study, out of the total sample of 65 objects studied by Rampazzo et al. (2005), Annibali et al. (2006), and Annibali et al. (2007), we have taken 15 early-type galaxies for which the *GALEX* measurements are already to disposal. In total we consider a sample of 18 galaxies. All relevant data are summarized in Tables 4 and 5.

Table 4 lists the total FUV, NUV and V magnitudes, the colour ($B-V$), the central velocity dispersion σ_c in km s^{-1}, the effective radius r_e in arcsec, and the colour (FUV$-$NUV)$_{r_e/8}$ (see below for the meaning of the suffix). Table 5 lists the values of line-strength indices that are customarily considered to be more sensible either to the age (e.g. Hβ, Hγ, Hδ) or the metallicity (e.g. Mg2). They are measured within an aperture centred on the nucleus of the galaxy with radius $r_e/8$ (the effective radius, r_e, contains half of the total galaxy light calculated in the *B*-band). Finally we list the age and metallicity assigned to each galaxy by Rampazzo et al. (2005), Annibali et al. (2006), and Annibali et al. (2007) as the most likely solution in the (age, Z, and [α/Fe]) space.

There is an important consideration to be made about the 'sensitivity' of the indices to the three most important parameters (age, metallicity, and degree of α-enhancement). The subject has been recently addressed by Tantalo & Chiosi (2004b) from a quantitative point of view. Limiting the discussion to Hβ and Mg2, the situation is as follows: Hβ strongly depends on all the three parameters with little resolving power; Mg2 primarily depends on metallicity and age, little on the degree of enhancement. For details see table 5 of Tantalo & Chiosi (2004b). This may explain part of the difficulties we have encountered with some galaxies in the discussion below.

Using these data we look for significant correlations between the *GALEX* (FUV$-$NUV)$_{r_e/8}$ colour measured within $r_e/8$ and the line-strength indices and compare them with theoretical predictions. To this aim we need to generate integrated magnitudes and colours of single stellar populations (SSPs) with different chemical compositions in the *GALEX* passbands.

5.3 Modelling *GALEX* magnitudes and colours

In the following, we briefly summarize the key assumptions and features of the stellar models and isochrones, library of stellar spectra and the ABmag photometric system that are used to calculate theoretical FUV and NUV magnitudes for SSPs.

(i) *Stellar models and isochrones.* We have adopted the Padova Library of stellar models and companion isochrones according to the release by Girardi et al. (2000) and Girardi (private communication). This particular set of stellar models/isochrones differs from the classical one by Bertelli et al. (1994) for the efficiency of convective overshooting and the prescription for the mass-loss rate along the AGB phase. The stellar models extend from the zero-age main-sequence up to either the start of the thermally pulsing AGB phase

Table 4. Data for the sample of 18 galaxies examined in this study. Columns (1)–(8) list the galaxy identification, the total FUV, NUV and V magnitudes, the total central colour $(B-V)_{tc}$, the central velocity dispersion σ_c in km s^{-1}, the effective radius r_e in arcsec, and the colour (FUV$-$NUV) within $r_e/8$.

Galaxy identifier	NUV total	FUV total	V total	$(B-V)_{tc}$	$\log\sigma_c$ (km s^{-1})	r_e (arcsec)$_{r_e/8}$	(FUV$-$NUV)
NGC 777	17.19 $\pm$ 0.01	17.70 $\pm$ 0.02	11.26 $\pm$ 0.14	0.87 $\pm$ 0.02	2.51 $\pm$ 0.01	34.4	0.20 $\pm$ 0.23
NGC 1052	15.83 $\pm$ 0.01	16.85 $\pm$ 0.01	10.34 $\pm$ 0.13	0.79 $\pm$ 0.01	2.32 $\pm$ 0.01	33.7	0.41 $\pm$ 0.22
NGC 1380	15.29 $\pm$ 0.01	16.78 $\pm$ 0.01	9.83 $\pm$ 0.10	0.80 $\pm$ 0.01	2.35 $\pm$ 0.01	20.3	0.83 $\pm$ 0.29
NGC 1389	16.78 $\pm$ 0.01	18.63 $\pm$ 0.02	11.42 $\pm$ 0.13	0.79 $\pm$ 0.01	2.14 $\pm$ 0.03	15.0	1.37 $\pm$ 0.22
NGC 1407	14.93 $\pm$ 0.01	15.64 $\pm$ 0.01	9.40 $\pm$ 0.20	0.84 $\pm$ 0.01	2.44 $\pm$ 0.01	70.3	0.19 $\pm$ 0.22
NGC 1426	16.84 $\pm$ 0.03	18.30 $\pm$ 0.08	11.29 $\pm$ 0.05	0.76 $\pm$ 0.01	2.19 $\pm$ 0.01	25.0	1.02 $\pm$ 0.59
NGC 1453	17.03 $\pm$ 0.06	18.16 $\pm$ 0.12	11.13 $\pm$ 0.13	0.83 $\pm$ 0.01	2.48 $\pm$ 0.03	25.0	0.80 $\pm$ 1.20
NGC 1521	17.15 $\pm$ 0.33	18.66 $\pm$ 0.11	11.24 $\pm$ 0.06	0.81 $\pm$ 0.01	2.38 $\pm$ 0.02	25.5	0.15 $\pm$ 0.49
NGC 1553	14.53 $\pm$ 0.01	16.18 $\pm$ 0.01	9.31 $\pm$ 0.08	0.75 $\pm$ 0.01	2.25 $\pm$ 0.01	65.6	1.24 $\pm$ 0.22
NGC 2865	16.93 $\pm$ 0.01	19.15 $\pm$ 0.04	11.34 $\pm$ 0.14	0.71 $\pm$ 0.01	2.26 $\pm$ 0.02	12.5	2.52 $\pm$ 0.28
NGC 4374	14.35 $\pm$ 0.01	15.60 $\pm$ 0.01	8.93 $\pm$ 0.05	0.82 $\pm$ 0.01	2.45 $\pm$ 0.01	50.9	0.59 $\pm$ 0.22
NGC 4552	14.83 $\pm$ 0.01	15.73 $\pm$ 0.01	9.57 $\pm$ 0.05	0.82 $\pm$ 0.01	2.42 $\pm$ 0.01	29.3	$-$0.05 $\pm$ 0.22
NGC 5018	16.45 $\pm$ 0.08		10.40 $\pm$ 0.13	0.71 $\pm$ 0.01	2.38 $\pm$ 0.02	22.8	1.05 $\pm$ 0.75
NGC 5638	16.27 $\pm$ 0.01	17.92 $\pm$ 0.02	11.04 $\pm$ 0.14	0.79 $\pm$ 0.01	2.22 $\pm$ 0.01	28.0	0.86 $\pm$ 0.29
NGC 5813	15.99 $\pm$ 0.01	17.10 $\pm$ 0.02	10.23 $\pm$ 0.13	0.81 $\pm$ 0.01	2.38 $\pm$ 0.01	57.2	0.77 $\pm$ 0.25
NGC 6958	16.42 $\pm$ 0.01	18.40 $\pm$ 0.04	11.22 $\pm$ 0.13	0.75 $\pm$ 0.01	2.28 $\pm$ 0.02	19.8	1.51 $\pm$ 0.27
NGC 7135	17.02 $\pm$ 0.01	18.44 $\pm$ 0.02	11.58 $\pm$ 0.10	0.84 $\pm$ 0.01	2.36 $\pm$ 0.02	31.4	$-$0.03 $\pm$ 0.23
IC 1459	15.58 $\pm$ 0.02	16.49 $\pm$ 0.04	9.89 $\pm$ 0.15	0.85 $\pm$ 0.01	2.49 $\pm$ 0.01	34.4	0.43 $\pm$ 0.22

Note. The values of (FUV$-$NUV) have been corrected for foreground extinction (Schlegel, Finkbeiner & Davies 1998).

Table 5. Line-strength indices within $r_e/8$ and age and metallicity assignments for the sample of 18 galaxies listed in Table 4.

Galaxy identifier	Hβ ($r_e/8$)	HγA ($r_e/8$)	HδA ($r_e/8$)	Mg2 ($r_e/8$)	Age (Gyr)	Z
NGC 777	1.48 ± 0.80	-5.340 ± 0.803	-3.080 ± 0.585	0.336 ± 0.013	5.4 ± 2.1	0.024 ± 0.004
NGC 1052	3.21 ± 0.09	-7.960 ± 0.143	-3.250 ± 0.109	0.335 ± 0.003	14.5 ± 4.2	0.032 ± 0.007
NGC 1380	1.75 ± 0.09	-5.570 ± 0.111	-2.740 ± 0.102	0.306 ± 0.002	4.4 ± 0.7	0.038 ± 0.006
NGC 1389	1.80 ± 0.10	-5.490 ± 0.127	-2.230 ± 0.113	0.286 ± 0.003	4.5 ± 0.6	0.032 ± 0.005
NGC 1407	1.62 ± 0.11	-6.290 ± 0.139	-3.330 ± 0.132	0.345 ± 0.003	8.8 ± 1.5	0.033 ± 0.005
NGC 1426	1.64 ± 0.09	-5.810 ± 0.129	-3.010 ± 0.116	0.285 ± 0.003	9.0 ± 2.5	0.024 ± 0.005
NGC 1453	1.59 ± 0.10	-5.840 ± 0.136	-3.510 ± 0.122	0.326 ± 0.003	9.4 ± 2.1	0.033 ± 0.007
NGC 1521	1.67 ± 0.10	-5.210 ± 0.144	-2.460 ± 0.122	0.284 ± 0.003	3.2 ± 0.4	0.037 ± 0.006
NGC 1553	1.90 ± 0.09	-5.790 ± 0.112	-2.780 ± 0.948	0.287 ± 0.002	4.8 ± 0.7	0.031 ± 0.004
NGC 2865	3.12 ± 0.15			0.209 ± 0.003	1.8 ± 0.5	
NGC 4374	1.75 ± 0.16	-6.170 ± 0.226	-2.670 ± 0.129	0.314 ± 0.005	9.8 ± 3.4	0.025 ± 0.010
NGC 4552	1.29 ± 0.13	-6.550 ± 0.152	-3.180 ± 0.155	0.341 ± 0.004	6.0 ± 1.4	0.043 ± 0.012
NGC 5018	2.68 ± 0.15			0.209 ± 0.003	2.8 ± 0.0	
NGC 5638	1.62 ± 0.14	-6.190 ± 0.203	-3.010 ± 0.170	0.308 ± 0.005	9.1 ± 2.3	0.024 ± 0.008
NGC 5813	1.78 ± 0.09	-6.280 ± 0.119	-3.070 ± 0.110	0.301 ± 0.002	11.7 ± 1.6	0.018 ± 0.002
NGC 6958	2.17 ± 0.09	-4.190 ± 0.121	-0.997 ± 0.110	0.258 ± 0.003	3.0 ± 0.3	0.038 ± 0.006
NGC 7135	2.41 ± 0.07	-6.390 ± 0.100	-3.630 ± 0.084	0.292 ± 0.002	2.4 ± 0.4	0.047 ± 0.010
IC 1459	1.70 ± 0.10	-6.900 ± 0.121	-3.630 ± 0.120	0.343 ± 0.003	8.0 ± 2.2	0.042 ± 0.009

Notes. The age of NGC 2865 is derived from the analysis of Hβ and [Ca II] indices by Longhetti et al. (1999) and Longhetti et al. (2000). For NGC 5018 we adopt the age estimated by Leonardi & Worthey (2000) on the basis of [Ca II] and Hδ/λ4005 line-strength indices. For both galaxies, the Hβ and Mg2 line-strength indices are taken from Longhetti et al. (2000).

Table 6. Chemical composition for the SSPs in use.

Z	Y	X
0.008	0.248	0.7440
0.019	0.273	0.7080
0.040	0.320	0.6400
0.070	0.338	0.5430

(TP-AGB) or carbon ignition. No details on the stellar models are given here; they can be found in Girardi et al. (2000) and Girardi et al. (2002). Suffice it to mention that: (i) in low mass stars passing from the tip of red giant branch (T-RGB) to the HB or clump, mass-loss by stellar winds is included according to the Reimers (1975) rate with $\eta = 0.45$; (ii) the whole TP-AGB phase is included in the isochrones with ages older than 0.1 Gyr according to the algorithm of Girardi & Bertelli (1998) and the mass-loss rate of Vassiliadis & Wood (1993); and (iii) four chemical compositions are considered as listed in Table 6.

(ii) *Library of stellar spectra.* The library of stellar spectra is taken from Girardi et al. (2002). It covers a large range of the $\log T_{\rm eff}$ – $\log g$–[M/H] space. No details are given here. Suffice to mention

(1) The basic spectra are from Kurucz ATLAS9 non-overshooting models (Castelli, Gratton & Kurucz 1997; Bessell, Castelli & Plez 1998) complemented with:

(2) Blackbody spectra for $T_{\rm eff} > 50,000$ K;

(3) Fluks et al. (1994) empirical M-giant spectra, extended with synthetic ones in the IR and UV, and modified shortwards of 4000 Å so as to produce reasonable $T_{\rm eff} - (U - B)$ and $T_{\rm eff} - (B - V)$ relations for cool giants;

(4) Allard et al. (2000) DUSTY99 synthetic spectra for M, L and T dwarfs.

Using the above library of stellar models and spectra, we have calculated the SSPs integrated spectra following the method described in Bressan et al. (1994).

It is worth recalling here that above a certain value of the metallicity, say $Z = 3\,Z_\odot$, these SSP exhibit the UV excess caused by the so-called AGB manqué stars of high metal content, whose percentage in the stellar population mix of a galaxy is small but high enough to give rise to the UV-upturn (see Bressan et al. 1994, for all details).

The theoretical absorption-line indices in the Lick system have been calculated as described in Tantalo & Chiosi (2004a,b, section 4) with the aid of the fitting functions given by Worthey et al. (1994) and Worthey & Ottaviani (1997).

The theoretical magnitudes used in this study have been calculated in the ABmag system (see Oke 1974) for the Johnson–Cousins–Glass *UBVRIJHK* system, using filter response curves from Bessell & Brett (1988) and Bessell (1990) and for the two bands (FUV and NUV) of *GALEX*[2] as described below.

(iii) *The ABmag system.* If the spectral flux as it arrives at the Earth, f_λ, is known, the apparent magnitude m_{S_λ}, in a given passband with transmission curve S_λ in the interval $[\lambda_1, \lambda_2]$, can be calculated by

$$m_{S_\lambda} = -2.5 \log \left(\frac{\int_{\lambda_2}^{\lambda_2} \lambda\, f_\lambda S_\lambda \mathrm{d}\lambda}{\int_{\lambda_2}^{\lambda_2} \lambda\, f_\lambda^0 S_\lambda \mathrm{d}\lambda} \right) + m^0_{S_\lambda}, \quad (1)$$

where f_λ^0 represents a reference spectrum (not necessary a stellar one) that produces a known apparent magnitude $m^0{}_{S_\lambda}$, Here, both f_λ^0 and $m^0{}_{S_\lambda}$, completely define the 'zero-points' of a synthetic photometric system.

By photometric 'zero-points', one usually means the constant quantities that one should add to instrumental magnitude in order to transform them to standard magnitudes, for each filter S_λ. In the formalism adopted here, we do not make use of the concept of instrumental magnitude, and hence such constants do not need to be defined, and we consider as 'zero-points' the quantities in

[2] The whole library of SSP models can be found on the website http://dipastro.pd.astro.it/galadriel/

equation (1) that depend only on the choice of f^0_λ and $m^0{}_{S_\lambda}$, which are constant for each filter.

In the original work by Oke (1964), monochromatic AB magnitudes are defined by

$$m_{\mathrm{AB},\nu} = -2.5 \log f_\nu - 48.60. \quad (2)$$

This means that a reference spectrum of constant flux density per unit frequency

$$f^0_{\mathrm{AB},\nu} = 3.361 \times 10^{-20} \,(\mathrm{erg\ s^{-1}\ cm^{-2}\ Hz^{-1}}) \quad (3)$$

will have AB magnitudes $m^0_{\mathrm{AB},\nu} = 0$ at all frequencies ν.

This definition can be extended to any filter system, provided that we replace the monochromatic flux f_ν with the photon counts over each passband S_λ obtained from the star, compared to the photon counts that one would get by observing $f^0_{\mathrm{AB},\nu}$:

$$m_{\mathrm{AB},S_\lambda} = -2.5 \log \left[\frac{\int_{\lambda_2}^{\lambda_2} (\lambda/hc)\, f_\lambda S_\lambda \,\mathrm{d}\lambda}{\int_{\lambda_2}^{\lambda_2} (\lambda/hc)\, f^0_{\mathrm{AB},\lambda} S_\lambda \,\mathrm{d}\lambda} \right], \quad (4)$$

where $f^0_{\mathrm{AB},\lambda} = f^0_{\mathrm{AB},\nu}\, c/\lambda^2$. It is easy to show that equation (4) is just a particular case of the most general equation (1) for which $f^0_{\mathrm{AB},\nu}$ is the reference spectrum given by equation (3), and $m^0{}_{\mathrm{AB}}, S_\lambda = 0$ are the reference magnitudes.

5.4 Comparing data with theory

The comparison of data with theory is made assuming that the complex stellar mix of a real galaxy can be reduced to a SSP of suitable metallicity and age. However, this approximation has different implications for the two parameters. While the metallicity distribution can be 'reasonably' approximated to the mean value, the same does not hold for the age, when this derived from integrated properties (see e.g. Serra & Trager 2007). In the discussion below, one has to keep in mind that the age we are measuring from colours and indices is always biased by the last episode of SF. In other words, it is a mean luminosity-weighted age, in which the most recent star-forming episode dominates at least during the first 2–3 Gyr from its occurrence. This is simply due to the rather well established law of luminosity fading of stellar populations, which ultimately mirrors the lifetime and evolutionary rate of a star as a function of its mass. In the following, we will refer to this age as T_{SF}. It does not necessarily coincide with the real age of a galaxy T_{G}. In general, if a galaxy underwent an initial star-forming episode ever since followed by quiescence, $T_{\mathrm{SF}} \simeq T_{\mathrm{G}}$; if later episodes of SF occurred, $T_{\mathrm{SF}} < T_{\mathrm{G}}$, the difference getting larger as the secondary activity gets closer to us in time. An old galaxy, may look young if secondary SF activity took place in the "recent past". We will come back to this in more detail later on.

The correlations we have been looking at are displayed in panels (a)–(h) of Fig. 10 in which the galaxies of Table 4 and 5 and the theoretical predictions are compared. Among the 18 galaxies under examination, we label the three of the present study and NGC 1553, NGC 6958, and NGC 1052, which deserve particular attention.

According to Annibali et al. (2007) NGC 1553 has a luminosity-weighted age T_{SF} of about 4.8 ± 0.7 Gyr and a metallicity of $Z = 0.031 \pm 0.004$. The colour $(\mathrm{FUV}-\mathrm{NUV})_{r_e/8}$ for this galaxy is 1.24 ± 0.22. Rampazzo et al. (2003) found that ionized gas is present in the centre of this galaxy. The kinematics shows that the ionized gas has a nearly regular velocity field suggesting that, if it was acquired from outside, the gas had time to settle down on to a small disc.

NGC 6958 belongs to the Malin & Carter (1983) list of southern shell early-type galaxies. Saraiva, Ferrari & Pastoriza (1999) show that the galaxy does not show any significant signature of interaction in the elliptically shaped isophotes. They conclude that, if the galaxy underwent a merger, the companion galaxy has probably already merged. According to Annibali et al. (2007) the average age T_{SF} of the galaxy in the central part is about 3.0 ± 0.3 Gyr and the metallicity is about two times solar ($Z = 0.038 \pm 0.006$).

Finally, the giant elliptical NGC 1052 is a well known optical LINER with an obscured active galactic nucleus (AGN) (see e.g. Terashima et al. 2002).

In the $(\mathrm{FUV}-\mathrm{NUV})_{r_e/8}$ versus $(B-V)_{\mathrm{tc}}$ plane (Fig. 10, panel a), the galaxies of our sample share the same distribution of *normal* early-type galaxies and shell galaxies are among the bluest objects (see e.g. Donas et al. 2006). The distributions of galaxies in the planes $(\mathrm{FUV}-\mathrm{NUV})_{r_e/8}$ versus the central velocity dispersion σ_{c} and Mg2 index (Fig. 10, panels b and c, respectively) are consistent with those reported for Virgo early-type galaxies in table 1 of Boselli et al. (2005).

In the plane $(\mathrm{FUV}-\mathrm{NUV})_{r_e/8}$ versus H_β (panel e of Fig. 10), shell galaxies appear to be peculiar. They indeed have quite high $\mathrm{H}\beta$ values suggesting the presence of young stellar populations. However, only NGC 7135 has also a rather blue $(\mathrm{FUV}-\mathrm{NUV})_{r_e/8}$ colour. The case of NGC 1052 showing also a high $\mathrm{H}\beta$ is probably connected with the LINER/AGN nature of this elliptical galaxy: its $\mathrm{H}\beta$ line-strength index is objectively difficult to be corrected for emission line 'infilling' (see also Annibali et al. 2007). In this sense, the shift towards high $\mathrm{H}\beta$ of NGC 2865 and NGC 7135 could *partly* suffer the problem of a (over)correction of the line-strength index, although,most of the galaxies plotted in Fig. 10 have emission lines in their spectra (see also Rampazzo et al. 2005; Annibali et al. 2006).

In the planes $(\mathrm{FUV}-\mathrm{NUV})_{r_e/8}$ versus $\mathrm{H}\gamma$ and $\mathrm{H}\delta$, shown in panels *f* and *g* of Fig. 10, where corrections are expected to be lower, shell galaxies more closely follow the trend and position predicted by the theoretical models.

According to the literature, all shell galaxies in our sample likely had a secondary, recent burst of SF in their nuclei. For NGC 2865 Longhetti et al. (1999, 2000) obtained an average age estimate T_{SF} for this star episode of about 2 Gyr both from $\mathrm{H}\beta$ and from the Ca II[H+K] indices. A similar age $T_{\mathrm{SF}}(2.2 \pm 0.4$ Gyr) is attributed to NGC 7135 by Annibali et al. (2007) as a consequence of its Balmer line-strength indices and metallicity higher than 2 times solar ($Z = 0.047 \pm 0.010$). Although these two galaxies should have the same T_{SF} from line-strength indices, they are located in the age–$(\mathrm{FUV}-\mathrm{NUV})_{r_e/8}$) plane at the two opposite extremes of the $(\mathrm{FUV}-\mathrm{NUV})_{r_e/8}$ values. Note, however, in Fig. 6 that NGC 7135 had a radial gradient in (FUV−NUV) moving from the centre to the outskirts where $(\mathrm{FUV}-\mathrm{NUV})_{r_e/8}$ is approximately 1-1.4. If NGC 7135 hosts a young stellar population, this is confined in the very centre of the galaxy. From the data shown in Fig. 5 there is no hint that the burst has occurred also in the shell.

Furthermore, in panels *d* and *h* of Fig. 10 we show the correlation between $(\mathrm{FUV}-\mathrm{NUV})_{r_e/8}$ and the age T_{SF} and the metallicity Z estimated by Annibali et al. (2007) from the data within $r_e/8$ area. Note that NGC2865 is missing because Longhetti et al. (2000) did not derive the metallicity of this object. All the galaxies in our sample span large ranges of metallicity (Z between 0.018 and 0.05) and ages T_{SF} (between 2 and 14 Gyr). NGC 7135 is very peculiar because a high metallicity and a young *Age* have been estimated for this object: indeed it is the galaxy with the largest discrepancy from the theoretical expectation.

Fig. 11 shows the plane (FUV−V) and (NUV−V) versus Mg2 and the comparison between theory and data. The line-strength index Mg2 of each galaxy is derived in the $r_e/8$ aperture, whereas the

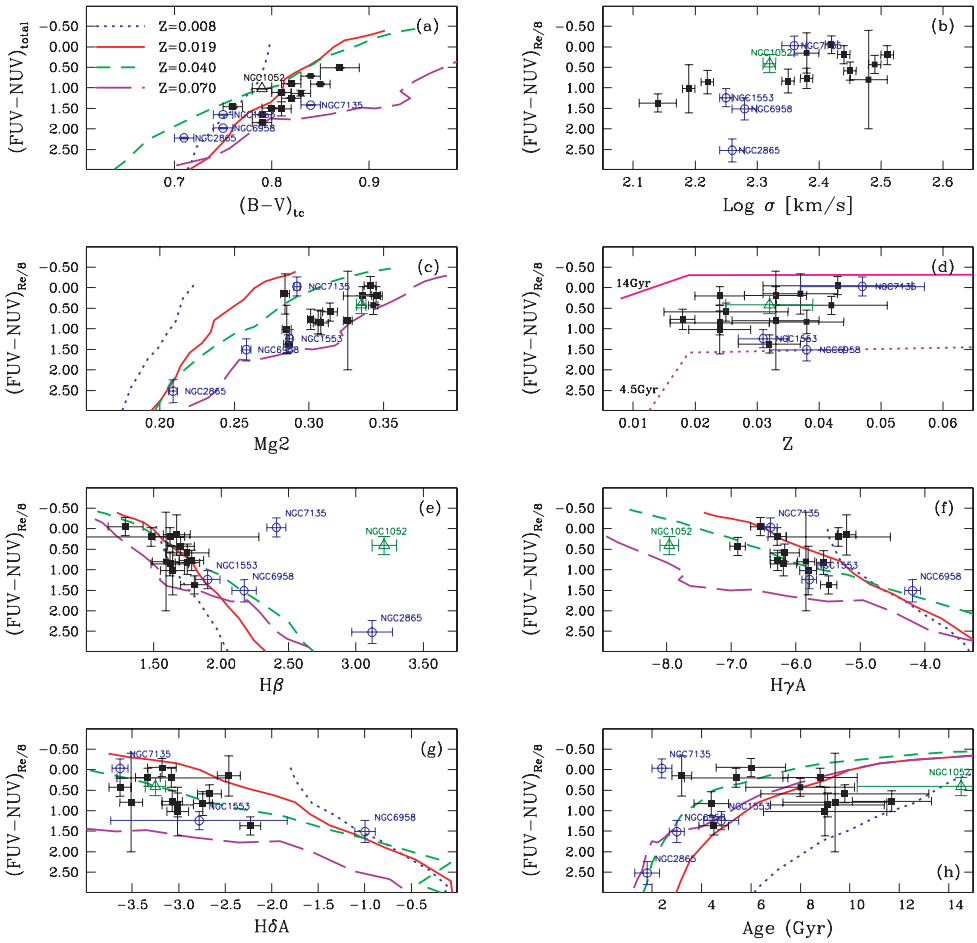

Figure 10. Panel (a): *GALEX* total (FUV−NUV) colour versus corrected total ($B-V$) colour. (FUV−NUV) colour within an aperture of $r_e/8$ radius versus central velocity dispersion (panel b), Mg2 line-strength index (panel c), Z (average galaxy metallicity) (panel d), Hβ (panel e), HγA (panel f), HδA (panel g) line-strength indices and the average age T_{SF} (panel h) estimated in the age–Z–[αFe] space (Annibali et al. 2007). Line-strength indices have been computed by Rampazzo et al. (2005) and Annibali et al. (2006). Lines in panels (a), (c), (d), (e), (g) and (h) report SSP models of different metallicities (solar metallicity $Z = 0.019$). In the $(FUV-NUV)_{r_e/8}$ versus H_β plane (panel e), the shell galaxies NGC 2865, NGC 7135 and NGC 1052 appear to be peculiar. They indeed have quite high Hβ values suggesting the presence of a young stellar population. The case of NGC 1052 is probably connected with the LINER/AGN nature of this elliptical galaxy: its Hβ line-strength index is objectively difficult to be corrected for emission line 'infilling' (see also Annibali et al. 2007). NGC 2865 and NGC 7135 could *partly* suffer the problem of an (over)correction of the Hβ line-strength index (see discussion in Section 5.4).

(FUV−V) and (NUV−V) colours refer to the whole galaxy. We are aware that this makes more difficult the comparison. Anyway, Annibali et al. (2007) found that, at least within $r_e/2$ there are no gradients in *age* and/or α-enhancements across the galaxies of their sample, whereas an average negative gradient in metallicity is firmly detected from the centre to $r_e/2$. In any case, Fig. 11 shows that a large spread for T_{SF} should exist and that the shell galaxies have the shortest values.

5.5 Simulating bursts of SF

(i) *Composite models with bursts*. The above comparison of data with theory has repeatedly strengthened the hint that at least part of the scatter in the various diagnostic planes could be due to recent episodes of SF (see Fig. 11 and panels d, e and h of Fig. 10). Not all diagnostic planes have the same power; however, the (FUV−NUV) versus Hβ plane (panel *e* of Fig. 10) deserves particular attention because of the peculiar position of NGC 7135, NGC 1052 and NGC 2865.

With the aid of the population synthesis technique we present simulations of composite stellar populations in which a recent burst of arbitrary intensity (mass percentage engaged in SF) and arbitrary age is superposed to an old stellar component with typical age of 10 Gyr and solar-like chemical composition. The simulations can also account for different metallicity between the old and newly born stars. All details of the technique in use can be found in Chiosi & Carraro (2002) and Tantalo & Chiosi (2004b).

Results of these simulations are shown in Fig. 12 in which is plotted the (*FUV* – *NUV*) colour versus Hβ within an aperture of $r_e/8$ radius. The lines describe the Age path induced by a recent burst of star superposed to a 10 Gyr old galaxy stellar population. The recovery time (i.e. the time elapsed from the beginning of the burst to the recover of the pre-burst situation, that is, colours, line indices, etc) of these simulations is about 2 Gyr or so. The analyses made by Chiosi & Carraro (2002) and Tantalo & Chiosi (2004b) show that the recovery time increases with the percentage of mass engaged in SF during the burst. Percentages above 20 per cent are not likely because the recovery time would be a significant fraction of the Hubble time and accordingly numerous galaxies could be caught in the bursting

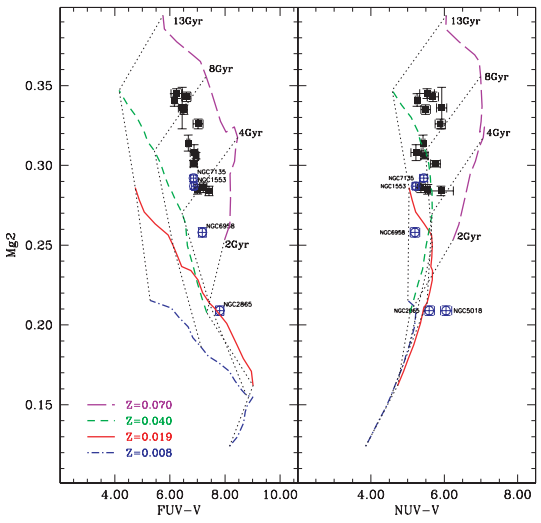

Figure 11. Comparison of the theoretical relation, Mg2 versus *GALEX* UV (FUV on the left-hand panel and NUV on the right-hand panel) – optical colours with our data.

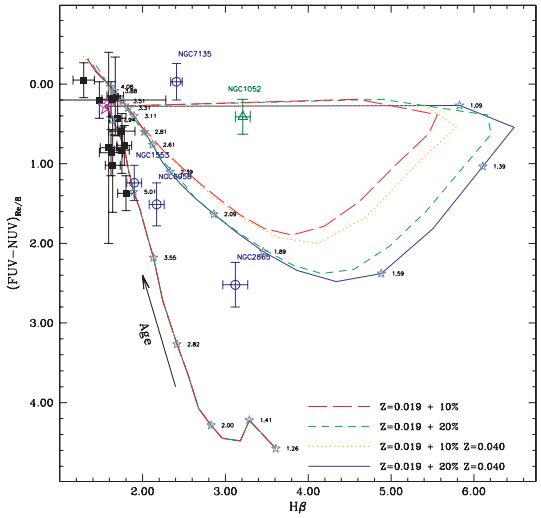

Figure 12. *GALEX* (FUV−NUV) colour versus Hβ within an aperture of an $r_e/8$ radius. In the above plane, the aging path of a galaxy stellar population is indicated by the arrow. The position of a 10-Gyr-old galaxy with a solar chemical composition is indicated by the large star located in the top left-hand part of the plot. A burst of SF, superposed on such an old stellar component, produces the 'closed paths' traced in the plot by the dotted, long-dashed, short-dashed and solid lines according to the percentage of the mass involved in the burst and of different metallicities in the newly born stars. The paths shown consider the percentages of 10 and 20 per cent of mass engaged in SF with a solar and two times solar metallicities. The time elapsed from the beginning of the burst is indicated along the solid line, tracing the path of a burst involving 20 per cent of the mass with two times solar chemical composition. In this context, the time elapsed from the burst of SF in NGC 7135 appears shorter than that in NGC 2865 and NGC 1553.

mode. See also Longhetti et al. (2000) for similar simulations and conclusions. In this context, the burst in NGC 7135 (and NGC 1052, see anyway the above notes about the nature of this galaxy) seems more recent than NGC 2865, NGC 6958 and NGC 1553. These latter are becoming *normal* ellipticals. Therefore, the anomalous position of the three galaxies in question can be explained.

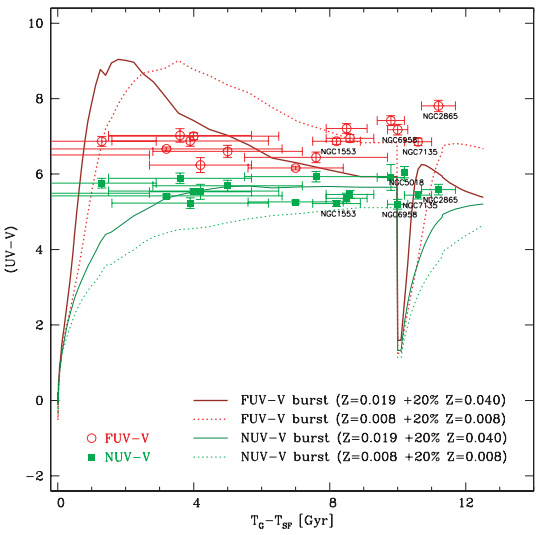

Figure 13. *GALEX* UV–optical colours of composite SSPs made by an old component and a more recent one as a function of the age. The age assigned to the real galaxies is $T_G - T_{SF} = 13 - T_{SF}$ (see the text). The shell galaxies of this paper are labelled. The burst occurs at the age of 10 Gyr, as in the previous figure. The four cases on display have the same burst intensity (20 per cent) but differ from the metallicity assigned to the young stars. The colour and symbol codes identify the UV–optical colour and the metallicity: the red open circles are for (FUV−V) and the green filled squares are for (NUV−V) of the observed galaxies. The heavy red solid line is for (FUV−V) of the model $Z = 0.019 +$ (20 per cent)0.04, the heavy red dotted line is for (FUV−V) of the model $Z = 0.008 +$ (20 per cent)0.008, the thin green solid line is for (NUV−V) of the model $Z = 0.019 +$ (20 per cent)0.04, and the thin green dotted line is for (NUV−V) of the model $Z = 0.008 +$ (20 per cent)0.008. Note the different recovery time and amplitude of the post-burst colour variation on changing metallicity.

(ii) *Anomalous position of a few objects in diagnostic planes*. It is also worth noting that the galaxies with anomalous position in Fig. 12 also have anomalous positions in panel *h* of Fig. 10. The situation is best illustrated in Fig. 13 (analogue of panel *h*) which correlates the (FUV−V) and (NUV−V) to the age. The models show the colour evolution with a recent burst of SF. The burst occurs at the age of 10 Gyr. The intensity of burst is 20 per cent and two possible combinations metallicity for the old and young components are shown. Of course, other values of the age at which the burst occurs, its intensity, and the chemical composition could be adopted. The age assigned to the observed galaxies is $T_G - T_{SF}$, where for T_G we adopt the canonical age of 13 Gyr. In other words all galaxies are supposed to initiate their SF history 13 Gyr ago. Therefore the plotted age is $13T_{SF}$ Gyr. The aim of this plot is to compare the observed properties of the galaxies in our sample with a typical SF history of a galaxy as suggested by the analysis carried out in the previous section. The choice of age at which the burst of SF occurred is suggested by the properties, that is, (FUV−NUV) colours and $H\beta$ indices of the shell galaxies. Attempts to reproduce other galaxies in the sample would require different assumptions for the burst age, but this is beyond the aims of this study.

At least the following five results can be inferred out of this comparison.

(i) In general the strongest variations of the colours are in coincidence of or soon after the star-forming episodes (the initial one, $T_{SF} \simeq T_G$, and the burst, $T_G - T_{SF} = 10$).

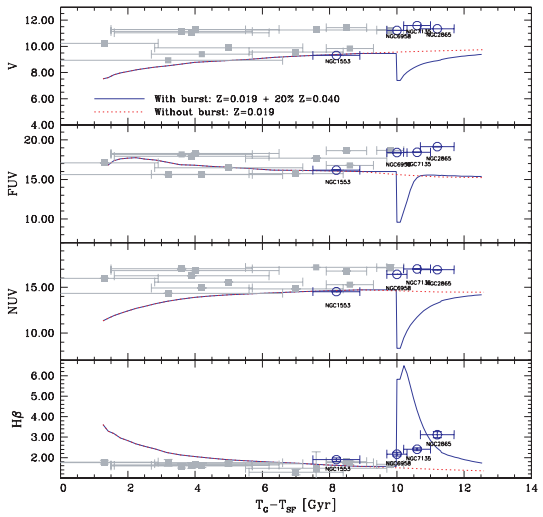

Figure 14. *GALEX* FUV, NUV, V magnitudes, and $H\beta$ index as a function of the age in a model galaxy evolved in quiescence (dotted lines). The theoretical FUV, NUV and V magnitudes have been rescaled to the faint-end boundary of the data (see the text). The thick symbols show the same quantities but for the model galaxy in which a recent burst of SF is added. The burst occurs at 10 Gyr. In this simulation, the original metal content is $Z = 0.019$, the mass fraction in the burst is 20 per cent and the metallicity of the newly born stars is $Z = 0.04$. The age plotted for the observed galaxies is $T_G - T_{SF}$ defined as in the previous plot.

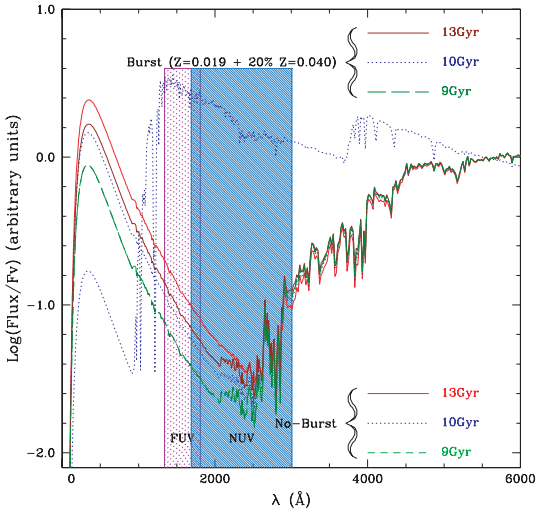

Figure 15. Spectral energy distributions as a function of the age (9, 10, 13 Gyr) for quiescent model galaxies (thin lines) and galaxies with a recent burst of SF (heavy lines). The burst occurs at 10 Gyr, and fades afterward. In this simulation, the original metal content is $Z = 0.019$, the mass fraction in the burst is 20 per cent and the metallicity of the newly born stars is $Z = 0.04$. The wavelength intervals for the *GALEX* FUV and NUV passbands are indicated by the two shaded areas.

(ii) The colour (FUV−NUV) is sensitive both to metallicity and to age over a long fraction of a galaxy life (see Fig 10, panel h);

(iii) The colour (NUV−V) (Fig. 13) soon becomes nearly age independent, say 2–3 Gyr past the star-forming activity both after the initial episode and after the burst. This time interval increases with the fractionary mass engaged in the star-forming episode: it is rather long in the initial episode (up to 4 Gyr) and only 1–2 Gyr after a burst of moderate intensity. It runs nearly flat during the long time interval between the two star-forming episodes (in this simulation) see also Yi et al. (2005) and Kaviraj et al. (2006). It keeps, however, some dependence on the metallicity, shifting to higher values at increasing Z;

(iv) The colour (FUV−V) (Fig. 13) keeps a good dependence on both age and metallicity all over the galaxy life;

(v) The anomalous location of the few shell galaxies under consideration correspond to the post-burst variations of the colour. By finely tuning the burst age, intensity and metallicity and the chemical composition of the old component we could easily match individual galaxies. This is beyond our present aims.

The temporal behaviour of the (FUV−V) and (NUV−V) colours as function of the age both in the pre-burst and in the post-burst regimes can be easily understood looking at the separate variation of the AB magnitudes FUV, NUV and V of our model galaxies with and without bursts of activity as a function of the age that are shown in the three top panels of Fig. 14 which does not require any additional explanation. The only thing to mention is that the magnitudes of the model galaxies (in reality composed SSPs) have been vertically shifted to make them nearly coincident with the observed ones. The vertical shift simply accounts for the difference between the luminous mass of the galaxies and the much smaller mass of the SSPs. The shift (the same for all passbands) is such that theoretical models and real data coincide at the faint end boundary of the data. In principle, an estimate of the mass could be derived from the velocity dispersion. However, as this would require some modelling of the relative mass in Dark and Baryonic Matter, we prefer to simply scale the magnitudes of the composite SSPs by a suitable amount. This is fully adequate to our purposes. Also in this case, the age adopted for the observed galaxies is $T_G - T_{SF} = 13 - T_{SF}$ Gyr. The agreement is fairly good. The shell galaxies on display can be associated to the post-burst period as the detection probability is higher thank to the slower fading rate. Perhaps they suggest some individual fine tuning of the burst age, which is, however, beyond our aims.

Finally in the bottom panel of Fig. 14 we show the temporal evolution of Hβ of the model galaxies with the observations. No vertical shift is now required (because the line strength indices are by definition mass independent). The age assigned to each real galaxy is the same as before. The agreement is remarkably good and the same remarks on the fine tuning of the burst age to fully match the shell galaxies could be made.

Which is the source of the FUV and NUV fluxes? The occurrence of a "rejuvenation" process in an early type galaxy by a recent burst of stars raises the issue of disentangling between the different sources (old and/or young stars) producing the FUV and NUV fluxes. Perhaps the best way of addressing this issue is to look at the SED of our model galaxies and its variation with time. This is shown in Fig. 15. A quiescent galaxy (of sufficiently high mean metallicity), during the time interval from 9 to 13 Gyr, changes its spectrum as shown by the thin lines in Fig. 15: at wavelengths longer than about 2500 Å little action occurs, whereas shortward of it the UV flux in the up-rising branch gets stronger. The slope of the up-rising branch below 2000 Å is nearly constant. Most likely, the source of this flux are the old hot-HB, and/or post-AGB, and the high-metallicity, AGB-manqué stars (see Bressan et al. 1994, for more details). The NUV region contains both flux from main-sequence (MS) turn-off stars of the evolved population (see e.g. Dorman, Rood & O'Connell 2003), perhaps independently of their extension across a galaxy, and flux from the UV-upturn. In contrast, the FUV

emission is due only to the evolved stars. In presence of a burst, the situation is more complicated. In the example shown in Fig. 15, we start with the spectrum at 9 Gyr exactly the same as the previous case, we jump to the spectrum dominated by the young component (heavy dotted line) at the time of the burst occurrence (10 Gyr), and then we nearly fall back to the previous case at the age of 13 Gyr. But for minor difference in the UV rising branch (shortwards of 2000 Å), the spectrum is the same as in the quiescent case (recovery of the old situation). The trace of the burst of stellar activity is limited to the minor difference in the flux of the rising branch. It is obvious that changing the age and the intensity of the burst many intermediate situations can be found in which the FUV and the NUV are more dominated by the recent burst of stellar activity. All this is of course mirrored by the colours and line strength indices in the typical diagnostic planes. Owing to the rapid fading of the burst, the probability of catching a galaxy during the maximum stellar activity so that the FUV and the NUV passbands are filled by radiation from the newly born stars is low compared to the probability of catching a galaxy either in the pre- or post-burst regime. This type of analysis holds its validity only in statistical sense. To conclude there is no unique answer to the question "which is the source of the FUV and NUV fluxes?" unless more information is provided.

6 SUMMARY AND CONCLUSIONS

We have presented the data for three early-type nearby galaxies (NGC 2685, NGC 5018 and NGC 7135) observed in the *GALEX* FUV and NUV passbands. These galaxies are characterized by prominent shell systems. The NUV emission of NGC 7135 and NGC 2685 mirrors the optical appearance and features. This implies that the UV emission comes from the same kind of stellar populations. The FUV images are instead more concentrated toward the nucleus in the case of NGC 2865 and/or in the case of NGC 7135 other particular regions of the galaxy thus suggesting that different types of hot stars contribute to the flux. In the case of NGC 5018, for which only the NUV image is available, it is not possible to reveal the shell structure visible in the optical, whereas the presence of a complex dust-lane system is seen.

All the galaxies show evidence of dust features in their centre. This confirms the trend found by Sikkema et al. (2007) who suggest that the dust detection rate in the shell ellipticals is significantly higher than in a 'normal' elliptical sample. Furthermore the irregular shape of shell galaxies suggests that external influences and/or acquisition of material are the cause of the dust features.

The three galaxies seem to belong to loose, poor groups rich of cold gas whose presence is traced by the H I emission. We suggest that these objects typically occur in *evolving groups* similar to the Arp 227 group dominated by the shell galaxy NGC 474 (Rampazzo et al. 2006). No galaxy of our sample shows the presence of cold gas in its innermost regions. In the case NGC 2865 Schiminovich et al. (1995) find that the outer cold gas is kinematically associated to the stellar body. This strongly suggests that whatever the phenomenon giving rise to the shells might be (the agreement between the gas and stellar kinematics somewhat rejects the merging hypothesis) it is able to convert the gas in the central regions into stars, thus 'rejuvenating' the galaxy in agreement with what inferred from the line-strength indices.

The analysis of the colour evolution of single and composite stellar populations simulating past and/or recent SF shows that (i) the colour (FUV−NUV) has good sensibility to metallicity and age over a long fraction of a galaxy life; (ii) The colour (NUV−V) soon becomes nearly age independent, say 2–3 Gyr past the star-forming activity both after the initial episode and after the burst. This time interval increases with the fractionary mass engaged in the star-forming episode. Thus, it is rather long in the initial episode (up to 4 Gyr) and only 1–2 Gyr after a burst of moderate intensity. It runs nearly flat during the long time interval between the two star-forming episodes (in this simulation). It keeps, however, some dependence on the metallicity shifting to higher values at increasing *Z*; (iv) finally, the colour (FUV−V) keeps a good dependence on both age and metallicity all over the galaxy life. In the typical case of secondary activity of moderate intensity, all the colours but for (FUV−NUV) and (FUV−V), become nearly age-insensitive when 1–2 Gyr have elapsed from the last star-forming episode (Jeong et al. 2007).

Most likely, the NUV and FUV fluxes of 'normal' early-type galaxies have different origins. Independently of its extension across a galaxy, the NUV flux is partially due to the MS turn-off stars of the evolved population (see e.g. Dorman et al. 2003) and partially to more evolved, exotic stars. In contrast, a strong FUV emission is likely due to the presence of one (or more) hot, plausibly high-metallicity, stellar components giving origin to the well-known phenomenon of the UV-upturn (e.g. hot-HB and/or post-AGB and AGB-manqué stars). Further complication comes from the analysis of the optical indices, which suggest that the three shell galaxies in our study had a recent (2–3 Gyr old) burst of stellar activity, possibly as a consequence of the interaction/accretion episode that triggered the shell formation. In this context, it comes naturally that the stellar populations should span a certain range of ages and also that young stars could be present in different proportions in both the NUV and the FUV fluxes. All this makes the interpretation of the data more difficult.

Our combined analysis of the (FUV−NUV) and (UV−V) colours and line-strength indices shows that even simple models such as SSPs mimicking the passive evolution of a galaxy can account for most of the gross features of shell galaxies as well as those of normal early-type galaxies. Among the shell galaxies in the sample, the nucleus of NGC 7135 shows the more peculiar behaviour when compared with theoretical expectation of passive evolution. Considering composite stellar population models with a recent burst of SF, we show that the position of the NGC 7135 nucleus in the (FUV−NUV)–Hβ plane could be explained in terms of a recent rejuvenation episode. NGC 2865 and the other few shell galaxies, which have a nearly 'normal' position in the above plane, could also fit the same rejuvenation framework.

Recently van Dokkum (2005) suggests that *dry* mergers, that is, nearly dissipationless, or gasless mergers, at low redshift are responsible for much of the local bright field elliptical galaxy population. Donovan, Hibbard & van Gorkom (2007) demonstrated that the morphological and photometric criteria adopted by van Dokkum (2005) to identify *dry* merger candidate could include early-type galaxies with H I in or around them, that is, possible *wet* ellipticals. The sample they considered is taken from the H I Rogues Gallery (Hibbard et al. 2001) and include NGC 2865, NGC 5018 and NGC 7135 which all fit the criteria for being *dry* mergers candidate. Our results suggest that the merger that has induced a secular evolution in NGC 7135 (and possibly in NGC 2865) should not have been so *dry*.

ACKNOWLEDGMENTS

This research has been partially founded by ASI-INAF contract I/023/05/0. *GALEX* is a NASA Small Explorer, launched in April

2003. *GALEX* is operated for NASA by California Institute of Technology under NASA contract NAS-98034. *GALEX* Guest Investigator program GALEXGI04-0030-0059. This research has made use of the NASA/IPAC Extragalactic Data base (NED) which is operated by the Jet Propulsion Laboratory, California Institute of Technology, under contract with the National Aeronautics and Space Administration. The Digitized Sky Survey (DSS) was produced at the Space Telescope Science Institute under U.S. Government grant NAG W-2166. The images of these surveys are based on photographic data obtained using the Oschin Schmidt Telescope at the Palomar Observatory and the UK Schmidt Telescope. The plates were processed into the present compressed digital form with the permission of these institutions.

REFERENCES

Aalto S., Hüttemeister S., 2000, A&A, 362, 42
Allard F., Hauschildt P. H., Alexander D. R., Ferguson J. W., Tamanai A., 2000, in Griffiths C. A., Marley M. S., eds, ASP Conf. Ser. Vol. 212, From Giant Planets to Cool Stars. Astron. Soc. Pac., San Francisco, p. 127
Annibali F., Bressan A., Rampazzo R., Zeilinger W. W., 2006, A&A, 445, 79
Annibali F., Bressan A., Rampazzo R., Danese L., Zeilinger W. W., 2007, A&A, 463, 455
Balcells M., van Gorkom J. H., Sancisi R., Del Burgo C., 2001, AJ 122, 1758
Barnes J., 1992, ApJ, 393, 484
Bertelli G., Bressan A., Chiosi C., Fagotto F., Nasi E., 1994, A&AS, 106, 275
Bertola F., Burstein D., Buson L. M., 1993, ApJ, 403, 573
Bessell M. S., 1990, PASP, 102, 1181
Bessell M. S., Brett J. M., 1988, PASP, 100, 1134
Bessell M. S., Castelli F., Plez B., 1998, A&A, 333, 231
Boselli A. et al., 2005, ApJ, 629, L29
Bressan A., Chiosi C., Fagotto F., 1994, ApJS, 94, 63
Burstein D., Bertola F., Buson L. M., Faber S. M., Lauer T. R., 1988, ApJ, 328, 440
Buson L. M., Bertola F., Cappellari M., Burstein D., 2001, in Funes S. J. J. G., Corsini E. M., eds, ASP Conf. Ser. Vol. 230, Galaxy Disks and Disk Galaxies. Astron. Soc. Pac., San Francisco, p. 435
Buson L. M., Bertola F., Bressan A., Burstein D., Cappellari M., 2004, A&A, 423, 965
Carollo C. M., Danziger I. J., 1994, MNRAS, 270, 743
Castelli F., Gratton R. G., Kurucz R. L., 1997, A&A, 318, 841
Charmandaris V., Combes F., van der Hulst J. M., 2000, A&A, 356, L1
Chiosi C., Carraro G., 2002, MNRAS, 335, 335
Colbert J. W., Mulchaey J. S., Zabludoff A., 2001, AJ, 121, 808
Davies R. L., Burstein D., Dressler A., Faber S. M., Lynden-Bell D., Terlevich R., Wegner G., 1987, ApJS, 64, 581
De Vaucouleurs G., de Vaucouleurs A., Corwin H. G., Jr, Buta R. J., Paturel G., Fouque P., 1991, Third Reference Catalogue of Bright Galaxies, Springer-Verlag, New York
Donas J. et al., 2006, ApJS, in press (astro-ph/0608594)
Donovan J. L., Hibbard J. E., van Gorkom J. H., 2007, AJ, 134, 118
Dorman B., Rood R. T., O'Connell, 2003, ApJ, 591, 878
Dupraz C., Combes F., 1986, A&AS, 166, 53
Ebeling H., White D. A., Rangarajan F. V. N., 2006, MNRAS, 368, 65
Fluks M. A., Plez B., The P. S., de Winter D., Westerlund B. E., Steenman H. C., 1994, A&AS, 105, 311
Fort B. P., Prieur J.-L., Carter D., Meatheringham S. J., 1986, ApJ, 306, 110
Gil de Paz A. et al., 2006, ApJS, in press (astro-ph/0606440)
Girardi L., Bertelli G., 1998, MNRAS, 300, 533
Girardi L., Bressan A., Bertelli G., Chiosi C., 2000, A&AS, 141, 371
Girardi L., Bertelli G., Bressan A., Chiosi C., Groenewegen M. A. T., Marigo P., Salasnich B., Weiss A., 2002, A&A, 391, 195
Hernquist L., Quinn P., 1987a, ApJ, 312, 1
Henquist L., Quinn P., 1987b, ApJ, 312, 17
Hernquist L., Spergel D. N., 1992, ApJ, 399, L117
Hernquist L., Mihos C., 1995, AJ, 110, 140
Hibbard J. E., van Gorkom J. H., Rupen M. P., Schiminovich D., 2001, in Hibbard J. E., Rupen M. P., van Gorkom J. H., eds, ASP Conf. Ser. Vol. 240, Gas and Galaxy Evolution. Astron. Soc. Pac., San Francisco, p. 657
Hibbard J. E. et al., 2005, ApJ, 619, L87
Kaviraj S. et al., 2006, ApJ, in press (astro-ph/0601029)
Keel C. W., 1985, AJ, 90, 2207
Kim D.-W., Guhathakurta P., van Gorkom J. H., Jura M., Knapp G. R., 1988, ApJ, 330, 684.
Kobayashi C., 2004, MNRAS, 347, 740
Jedrzejewski R., 1987, MNRAS, 226, 747
Jeong H., Bureau M., Yi S. K., Krainović D., Davies R., 2007, MNRAS, 376, 1021
Jørgensen I., Franx M., Kjægaard P., 1992, A&AS, 95, 489
Leonardi A. J., Whorthey G., 2000, ApJ, 534, 650
Longhetti M., Rampazzo R., Bressan A., Chiosi C., 1998, A&AS, 130, 267
Longhetti M., Bressan A., Chiosi C., Rampazzo R., 1999, A&A, 345, 419
Longhetti M., Bressan A., Chiosi C., Rampazzo R., 2000, A&A, 353, 917
Malin D., Carter D. F., 1983, ApJ, 274, 534
Martin D. C. et al., 2005, ApJ, 619, L1
Mattews L. D., van Driel W., 2000, A&AS, 143, 421
Merlin E., Chiosi C., 2006, A&A, 457, 437
Morrissey P. et al., 2005, ApJ, 619, L7
Oke J. B., 1964, ApJ, 140, 689
Oke J. B., 1974, ApJS, 27, 21
Peletier R. F., 1990, A&A, 233, 62
Peng C. Y., Ho L. C., Impey C. D., Rix H., 2002, AJ, 124, 266
Rampazzo R., Plana H., Longhetti M., Amram P., Boulesteix J., Gach J.-L., Hernandez O., 2003, MNRAS, 343, 819
Rampazzo R., Annibali F., Bressan A., Longhetti M., Padoan F., Zeilinger W. W., 2005, A&A, 433, 497
Rampazzo R. et al., 2006, MNRAS, 368, 851
Reduzzi L., Longhetti M., Rampazzo R., 1996, MNRAS, 282, 149
Reid N., Boisson C., Sansom A. E., 1994, MNRAS, 269, 713
Reimers D., 1975, Memoires of the Societe Royale des Sciences de Liege, 8, 369
Sansom A. E., Hibbard J. E., Schweizer F., 2000, AJ, 120, 1946
Saraiva M. F., Ferrari F., Pastoriza M. G., 1999, A&A, 350, 339
Schiminovich D., van Gorkom J. H., van der Hulst J. M., Kasow, S., 1994, ApJ, 423, L101
Schiminovich D., van Gorkom J. H., van der Hulst J. M., Malin D. F., 1995, ApJ, 444, L77
Schiminovich D., van Gorkom J. H., Dijkstra M., Li Y., Petric A., van der Hulst J. M., 2001, in Hibbard J. E., Rupen M. P., van Gorkom J. H., eds, ASP Conf. Ser. Vol. 240, Gas and Galaxy Evolution. Astron. Soc. Pac., San Francisco, p. 864
Schlegel D. J., Finkbeiner D. P., Davies M., 1998, ApJ, 500, 525
Schweizer F., 1990, ApJ, 364, L33
Schweizer F., 1992, in Danziger I. J., Zeilinger W. W., Kjär K., eds, Structure, Dynamics and Chemical Evolution of Elliptical galaxies, ESO/IPC, 651
Serra P., Trager S. C., 2007, MNRAS, 374, 769
Sersic J. L., 1968, Atlas de Galaxias Australes, Osservatorio Astronomico, Cordoba
Sikkema G., Carter D., Peletier R. F., Balcells M., del Burgo C., Valentijn E. A., 2007, A&A, 467, 1011
Tantalo R., Chiosi C., 2004a, MNRAS, 353, 405
Tantalo R., Chiosi C., 2004b, MNRAS, 353, 917
Terashima Y., Iyomoto N., Ho L. C., Ptak A. F., 2002, ApJS, 139, 1
Thomson R. C., 1991, MNRAS, 253, 256
Thomson R. C., Wright, 1990, MNRAS, 224, 895
Tully R. B., 1988, Nearby Galaxy Catalogue, Cambridge Univ. Press

van Dokkum P. G., 2005, AJ, 130, 2647
Vassiliadis E., Wood P. R., 1993, ApJ, 413, 641
Wilkinson A., Prieur J.-L., Lemoine R., Carter D., Malin D., Sparks W. B., 2000, MNRAS, 319, 977
Whitmore B. C., Lucas R. A., McElroy D. B., Steinman-Cameron T. Y., Sackett P. D., Olling R. P., 1990, AJ, 100, 1489
Worthey G., Faber S. M., Gonzalez J. J., Burstein D., 1994, ApJS, 94, 687
Worthey G., Ottaviani D. L., 1997, ApJS, 111, 377
Yi S. K. et al., 2005, ApJ, 619, L111

This paper has been typeset from a TEX/LATEX file prepared by the author.